MODELING OF MAGNETIC NON-LINEAR CHARACTERISTICS IN ELECTRIC MACHINES

By

Juan Carlos Garcia Alonso

A thesis submitted to

the Faculty of Graduate Studies

in Partial Fulfillment of the Requirements for the Degree of

MASTERS OF SCIENCE

Department of Electrical and Computer Engineering

UNIVERSITY OF MANITOBA

Winnipeg, MB, Canada

September 2005

THE UNIVERSITY OF MANITOBA

FACULTY OF GRADUATE STUDIES

*****

COPYRIGHT PERMISSION

Modeling of Magnetic Non-Linear Characteristics in Electric Machines

BY

Juan Carlos Garcia Alonso

A Thesis/Practicum submitted to the Faculty of Graduate Studies of The University of Manitoba in partial fulfillment of the requirement of the degree

Of

Master of Science

ACKNOWLEDGEMENTS

I would like to express my gratitude to my advisor Professor Ani Gole and to Dr. Dharshana Muthumuni for their support, guidance and suggestions throughout this work.

I would like to thank Robert and Malgorzata Yonza for their suggestions in reviewing this thesis, Ali Dehkordi for some valuable discussions and for allowing me to use his computer space in countless occasions, Magsoft for providing the Flux 2D/3D license of vital importance in this work and the HVDC Research Centre for granting me access to their facilities and equipment.

I must also thank Manitoba Hydro for providing the much needed financial support in my early days as a graduate student.

Lastly, my most special gratitude goes to my parents and my sisters.

ABSTRACT

Modeling magnetic non-linear characteristics of electromechanical systems usually represents a challenge for designers and engineers and often requires the use of rough approximations. Finite Element Analysis (FEA) coupled with Electromagnetic Transient Simulation Programs (ETSP) using time stepped field solutions can yield accurate results [2], however such approaches require long simulation times.

This paper explores the applicability of FEA and ETSP in a decoupled manner. For such purpose a model of the magnetic non-linear characteristics of a contactor is derived by means of multiple magneto-static FEA. This model is fed into the ETSP in the form of lookup tables where different time dependent scenarios are simulated. The same scenarios are simulated using the coupled transient electromagnetic-FEA engine. It is found that the decoupled approach yields closely comparable results to the transient FEA as long as the eddy currents do not play a key role in the application.

A three-phase power transformer is modeled using a non-linear lumped magnetic circuit. The performance of this model is compared against a 2D transient electromagnetic-FEA model for different levels of core magnetization in the steady state. The finding of this simulation is that the lumped method can yield accurate results for nominal levels of core magnetization.

Finally, a single-phase transformer model is created using two different kinds of non-linear lumped magnetic and electric circuits. These models are compared against a 2D FE axi-symmetric model for transitory events, namely energization events. It is found that the calculated inrush current and core flux density do not differ by more than 10% when the leakage flux is incorporated into the magnetic circuit as leakage reluctances.

TABLE OF CONTENTS

LIST OF FIGURES

LIST OF TABLES

NOMENCLATURE

FEA	finite elements analysis
ETSP	Electromagnetic transient simulation program
v	Voltage
L	Inductance
i	Current
t	Time
g	Conductance
$\overline{\nabla}\times$	Curl
$\overline{J}$	current density
$\overline{J}_S$	source current density
$\overline{J}_e$	induced current density
$\overline{J}_D$	displacement current density
$\overline{D}$	electric flux density
$\overline{B}$	flux density
$\overline{A}$	vector magnetic potential
μ	magnetic permeability
r_S	series resistance
r_C	coil resistance
2D	two-dimensional
3D	three-dimensional
emf	electromotive force

λ	flux linkage
m	Mass
a	Acceleration
k	spring constant
f_m	magnetic force
y	air gap distance
v	Velocity
b	friction coefficient
ρ	Resistivity
σ	Conductivity
v_{Hi}, v_{Xi}, v_{Yi},	voltage at circuit h, x or y (phase i)
n_i	coil i number of turns
ϕ	magnetic flux
L_σ	leakage flux
R	Reluctance
A	Area
RB	coil radial build
ID	coil inner diameter
h	coil height
Bn	nominal flux density
Lc	core length
$\mathbf{C}(t)$, $\mathbf{D}(t-\Delta t)$, $\mathbf{Q}(t)$, $\mathbf{F}^{sat}(t)$	matrices created in order to represent solutions in a simplified way

Note: bold symbols denote matrices

1 INTRODUCTION: SIMULATION TECHNIQUES

This thesis introduces a new high-speed method for simulating transients in electromagnetic systems with non-linear inductive components. This method combines Finite Element Analysis (FEA) and Electromagnetic Transient Simulation Programs (ETSP) in a decoupled manner. For such purpose, models of the system's non-linear inductive elements are initially mapped using multiple magneto-static FEA. These mapped models are then incorporated into the system's lumped RL circuit in the form of look-up tables. The circuit differential equations are finally solved in the time domain by systematically applying time stepped trapezoidal integrations (Dommel's method) [16].

Different cases were simulated using this technique and it was found that it yields very accurate results when compared against transient FEA. An advantage of this approach is that once the model of the non-linear electromagnetic system has been developed, it can be incorporated into very large electrical networks containing several other non-linear components. This network can then be simulated with standard ETSP software like PSCAD/EMTDC. This large-scale network of non-linear elements would otherwise be impossible to simulate using transient FEA.

This chapter provides a brief description of the two main simulation techniques used in this thesis, starting with Dommel's method and closing with FEA.

Chapter 2 explains the implementation of the decoupled method through a single-inductor example case. Chapter 3 evaluates the method's accuracy using as reference for comparison transient finite element simulations.

Chapter 4 explores the use of the decoupled method on a case of higher complexity, which involves the modeling of non-linear mutual inductances. It also introduces a technique developed to measure self and mutual inductances needed, very much need to create the inductance mapped model. The results of two different simulations devised to test the method's accuracy are presented.

Chapters 5 and 6 present two alternative approaches, which can be used to model non-linear electromagnetic devices whose complexity is too high for the decoupled method.

Finally, a series of conclusions and recommendations based on the findings of this thesis are given in the last chapter.

1.1 Simulation techniques

1.1.1 Dommel's Method

ETSP are computer applications that are applied to electrical networks and solve for transient voltages and currents in the time domain. There are several such applications

available on the market. The one used for the purpose of this thesis was PSCAD/EMTDC, based on Dommel's Method. [16]

Dommel's method, first introduced at the end of the 60's, models lumped inductors and capacitors as simple resistors paralleled with current sources through the use of the trapezoidal integration rule. This method simplifies complex network differential equations into a collection of, relatively easier to solve, linear equations.

The main philosophy of this approach can be illustrated with a simple example case: a single lumped inductance. The voltage differential equation of an ideal inductance is given by

$$V_L = L\frac{di(t)}{dt} \qquad \text{Eq. 1.1}$$

The solution to Eq. 1.1 needs to be found in terms of time steps so as to obtain an expression that can be implemented in a computer program. Hence, Eq. 1.1 is integrated between t-Δt and t as follows

$$\int_{t-\Delta t} V_L dt = L\int_{t-\Delta t} di \qquad \text{Eq. 1.2}$$

According to the trapezoidal rule (see Figure 1-1), the integral of a function $f(t)$ between t-Δt and t is given by

$$\int_{t-\Delta t} f(t)dt \approx \frac{f(t)+f(t-\Delta t)}{2}\Delta t \qquad \text{Eq. 1.3}$$

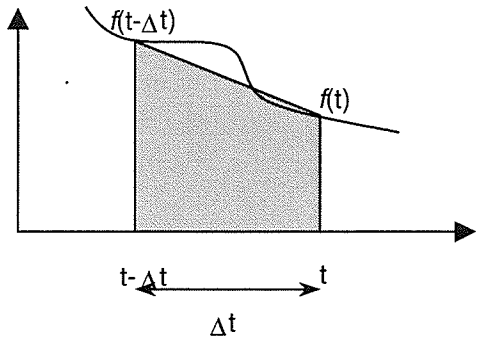

Figure 1-1 Trapezoidal rule

Therefore, applying Eq. 1.3 to Eq. 1.2 and solving for i(t) yields to the expression

$$i(t) \approx i(t-\Delta t) + \frac{\Delta t}{L}\frac{V(t)+V(t-\Delta t)}{2} \qquad \text{Eq. 1.4}$$

These type of expressions are usually written in terms of a history term i_h(t-Δt) which depends on past conditions and a term dependant on the present voltage across the variable inductance [6], as described by the following equation

$$i(t) \approx g_L V(t) + I_h(t-\Delta t) \qquad \text{Eq. 1.5}$$

where

$$g_L = \frac{\Delta t}{2L},$$

and

$$I_h(t-\Delta t) = i(t-\Delta t) + \frac{\Delta t}{2L}V(t-\Delta t)$$

Eq. 1.5 can be graphically represented as a conductance g_L in parallel with a current source $I_h(t-\Delta t)$ as follows

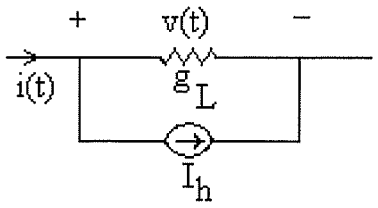

Figure 1-2 Equivalent circuit for variable inductors (valid during a time-step)

This treatment can be applied to several elements in the network. The system equations can then be reduced to a system of linear equations of the form

$$\mathbf{G} \cdot \mathbf{V} = \mathbf{I} \qquad \text{Eq. 1.6}$$

where the voltage vector $\mathbf{V}$ can be solved using one of many available numerical methods.

1.1.2 Finite Element Analysis

Analytical solutions to electromagnetic problems that involve field distributions across complex geometries can be very tedious and difficult if not impossible, especially if non-linear materials are involved. In fact, in most cases the only way to solve them is by means of numerical techniques.

Many numerical methods, such as finite differences, finite elements or boundary elements can be used in the solution of this kind of problem. Due to the relative

availability of FEM based commercial tools for electromagnetic analysis and their suitability for modeling non-linear materials, FEM was chosen for this thesis.

FEM divides the geometry to be studied into a finite number of ***elements*** that are connected by a series of joints or ***nodes*** (see Figure 1-3). The physical properties of each element are defined and the equations of equilibrium for the whole structure are solved, such that the continuity at each node is ensured taking into account the restrictions imposed by the boundary conditions [9] [10].

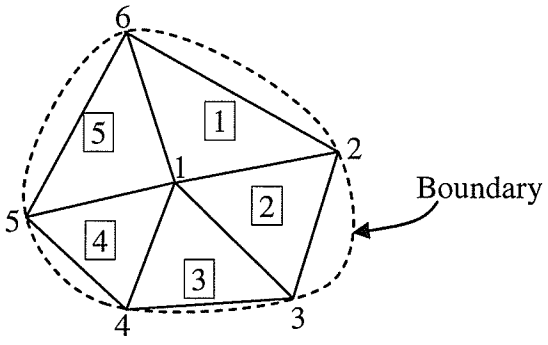

Figure 1-3 Typical finite element subdivision of a domain. [e] element No., ***n*** node No.

Electromagnetic FEA are usually based on the solution of Maxwell's third equation (see Appendix 1)

$$\vec{\nabla} \times \vec{H} = \vec{J} + \frac{\partial \vec{D}}{\partial t} \qquad \text{Eq. 1.7}$$

With loss of some generality, two-dimensional FEM modeling was utilized in this thesis.

The two dimensional solution to Eq. 1.7 is generally found in terms of the vector magnetic potential $\vec{A}$, which is defined by

$$\vec{B} = \vec{\nabla} \times \vec{A} \qquad \text{Eq. 1.8}$$

Inserting this equation into Eq. 1.7 then yields

$$\vec{\nabla} \times \left(\frac{1}{\mu} \vec{\nabla} \times \vec{A} \right) = \vec{J}_s + \vec{J}_e + \frac{\partial \vec{D}}{\partial t} \qquad \text{Eq. 1.9}$$

which is then solved by FEA.

Two different kinds of FEA were used: transient FEA and magneto-static FEA. Transient FEA takes into account time dependant events by solving Eq. 1.9 in full. Magneto-static FEA is time invariant, yielding null solutions for the displacement current density $\vec{J}_D = \partial \vec{D} / \partial t$ and induced current density $\vec{J}_e = -\sigma \, \partial \vec{A} / \partial t$. Hence the source's current density $\vec{J}_s$ becomes the only source of magnetic field, assuming that there are no permanent magnets or moving boundary charges present in the geometry.

The differential equation solved by the magneto-static FEA is then given by

$$\vec{\nabla} \times \left(\frac{1}{\mu} \vec{\nabla} \times \vec{A} \right) = \vec{J}_s \qquad \text{Eq. 1.10}$$

2 DEVELOPMENT OF THE FEA – ETSP DECOUPLED APPROACH

When modeling complex non-linear components, coupled transient FEA with ETSP can in general yield more accurate results than those derived from lumped circuit simulation techniques alone. However, such analysis may require prohibitive long simulation times.

The content of this and the next chapter are the fundamental new contribution of this thesis. They explore the use of FEA and ETSP in a decoupled manner in an effort to create a low complexity, yet accurate, model that can easily be incorporated into ETSP type models of very large electrical networks. The ETSP used to simulate the electromagnetic system studied in this and the next chapter was PSCAD/EMTDC.

In the decoupled FEA - ETSP method presented here, the electromagnetic system's non-linear characteristics are first modeled through multiple magneto-static finite element simulations, and then incorporated into the previously written electromagnetic transient model in the form of lookup tables.

The development of this new approach is presented in this chapter through a non-linear actuator example case: a translational contactor (shown in Figure 2-1).

Figure 2-2 shows the electrical network the contactor was connected to during the simulations carried out as part of this study. In this particular electrical network, the contactor was connected a DC voltage source E trough a switch S. The diode D allows

the current in the contactor's inductance to continue to flow (referred to as "free wheeling") whenever the switch is opened.

According to Figure 2-1, this contactor is composed mainly of three parts: coil, spring and core. The core is in turn composed of two subparts, a stationary part and a mobile part, also known as a blade.

When the contactor is de-energized or in its resting position (i.e., the switch has been left open for an extended period of time), the blade is held up by the spring a distance y away from the main body of the core. As the switch is closed, the increasing current flowing through the coil induces a magnetic flux, which flows through the core, blade and air-gap set. This flux creates a magnetizing force that acts in downward direction on the blade $\vec{a}_y$, closing the air-gap. Once the switch is reopened, the current flowing through the coil and the magnetizing force decay. The blade starts traveling back towards its initial position once the magnetic force becomes smaller than the upwards spring force.

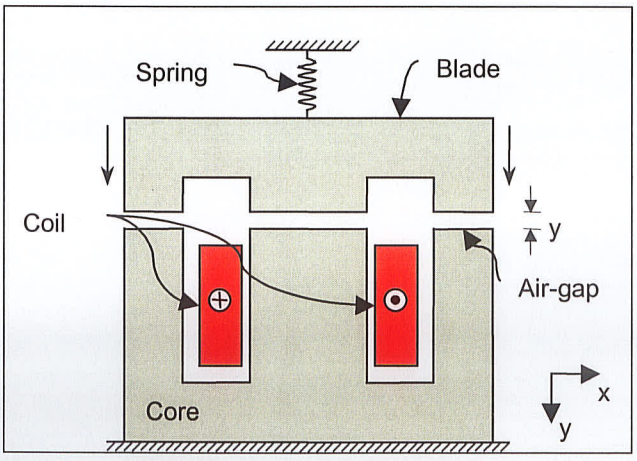

Figure 2-1 Two-dimensional representation of the contactor used in the simulation

The method used to analyze the electromagnetic system in Figure 2-1 consisted, in first instance, of representing the contactor as an R-L equivalent model in the ETSP environment.

With the system's electrical equations already formulated, the inductance value was tabulated as a function of current i and air-gap opening y using multiple magnetostatic FEA. The dynamic position $y(t)$ can be found by solving the mechanical equations of motion, which are also dependent on the magnetizing force f_m. The magnetic force f_m is a function of current i and position $y(t)$ and can also be tabulated using the FEA program as will be explained later.

Once the system's model was created, the problem was ready for implementation in an ETSP. A commercially available ETSP solver, PSCAD/EMTDC, was used to simulate the electrical network in Figure 2-2. This network was in turn used to test the method proposed here for accuracy and speed. Figure 2-3 provides a summary of the steps taken during the analysis of the contactor electromagnetic system.

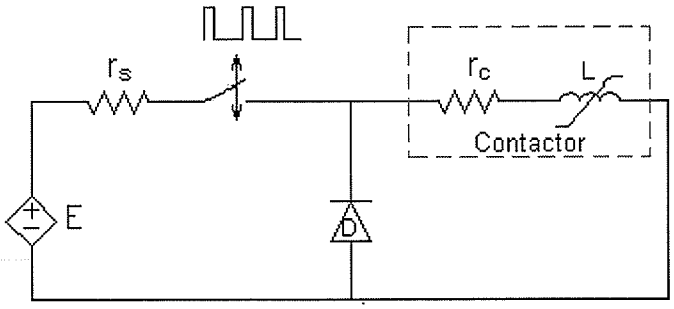

Figure 2-2 Equivalent lumped RL circuit

It is expected that the lumped RL approach with look-up table to be significantly faster than transient FEA. On the other hand, transient FEA should be more accurate because it can take into account some time dependant phenomena such as eddy currents, which are not incorporated into the decoupled model.

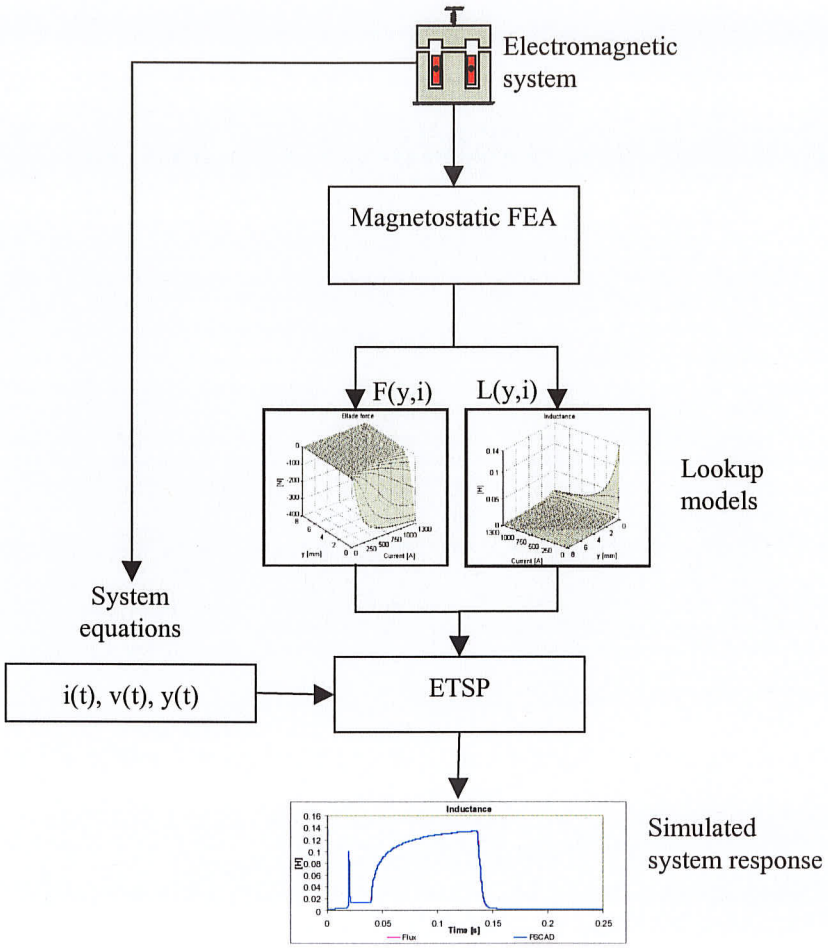

Figure 2-3 Steps carried out during the modeling and analysis of the contactor electromagnetic system

2.1 Mathematical modeling of the contactor

A low frequency lumped circuit for the contactor in Figure 2-1 can be given as a resistor in series with a variable inductor.

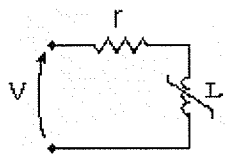

Figure 2-4 Variable inductance equivalent lumped RL circuit

The closed loop voltage equation for the element in Figure 2-4 is given by

$$V = ir + \frac{d}{dt}(Li) \qquad \text{Eq. 2.1}$$

According to Figure 2-1 the blade is affected by the spring force $-k\,y$, the magnetic force f_m and the friction $-b\,v$ (the weight is not taken into account since its effects are already cancelled by the spring's elongation at rest or initial position).

$$\sum f = ma = f_m - ky - b\,v \qquad \text{Eq. 2.2}$$

Summarizing, the contactor problem is described by the set of equations Eq. 2.1, Eq. 2.2 and the basic equations for velocity and acceleration given in Eq. 2.3

$$v = \frac{\partial y}{\partial t} \quad \text{and} \quad a = \frac{\partial v}{\partial t} \qquad \text{Eq. 2.3}$$

2.2 PSCAD modeling

2.2.1 Lumped electrical circuit model

In order to solve the system of differential equations mentioned above in the PSCAD environment, they must be written in terms of time step increments [6]. For this purpose, the trapezoidal approach introduced in the first chapter was used. This is very powerful because it allows for simulating very large electrical networks containing several non-linear magnetic elements, like the one modeled here. This would be otherwise practically impossible if using transient FE solvers alone. The inductance model is developed below in a manner similar to that for the linear inductor in Section 1.1.1.

In Eq. 2.1 the most right term represents the voltage V_L over and ideal variable inductor

$$V_L = \frac{\partial}{\partial t}(Li) \qquad \text{Eq. 2.4}$$

This expression can be reorganized and integrated between t-Δt and t, which yields

$$\int_{t-\Delta t} V_L dt = \int_{t-\Delta t} d(Li) \qquad \text{Eq. 2.5}$$

Applying Eq. 1.3 to Eq. 2.5 on the left side of the equation and integrating on the right side produces the following equation

$$\frac{\Delta t}{2}\left[V(t)+V(t-\Delta t)\right] = L(t)\,i(t) - L(t-\Delta t)\,i(t-\Delta t) \qquad \text{Eq. 2.6}$$

In this expression, the inductance at time t depends on the values of current $i(t)$ and blade position $y(t)$ at the present time step t, therefore, the solution of Eq. 2.6 for the current $i(t)$ is written as

$$i(t)=\frac{1}{L(y(t),i(t))}\frac{\Delta t}{2}V(t)+\frac{1}{L(y(t),i(t))}\left[L(t-\Delta t)i(t-\Delta t)+\frac{\Delta t}{2}V(t-\Delta t)\right] \qquad \text{Eq. 2.7}$$

which is the final equation for the current at time t.

Following the procedure used in Section 1.1.1, Eq. 2.7 can be re-written in terms of present and history term, as follows

$$i(t) \approx g_L V(t) + I_h(t-\Delta t) \qquad \text{Eq. 2.8}$$

where

$$g_L = \frac{1}{L(y(t),i(t))}\frac{\Delta t}{2},$$

and

$$I_h(t-\Delta t)=\frac{1}{L(y(t),i(t))}\left[L(t-\Delta t)i(t-\Delta t)+\frac{\Delta t}{2}V(t-\Delta t)\right]$$

The previous equation can then be represented as a parallel resistance and current source as in Figure 1-2. The only difference with the linear inductor model of Section 1.1.1 is that here, the g_L value is updated every time step.

2.2.2 Mechanical model

The forces equation (see Eq. 2.2) can be reorganized and written for time step t as follows

$$f_m(t) = ky(t) + b\,v(t) + ma(t) \qquad \text{Eq. 2.9}$$

It can also be written for the previous time step $t - \Delta t$ as follows

$$f_m(t-\Delta t) = ky(t-\Delta t) + b\,v(t-\Delta t) + ma(t-\Delta t) \qquad \text{Eq. 2.10}$$

The average magnetic force during the time step $t - \Delta t \rightarrow t$ can be calculated by adding and dividing by two the two previous expressions, obtaining

$$\frac{f_m(t) + f_m(t-\Delta t)}{2} = k\frac{y(t) + y(t-\Delta t)}{2} + b\frac{v(t) + v(t-\Delta t)}{2} + m\frac{a(t) + a(t-\Delta t)}{2} \qquad \text{Eq. 2.11}$$

where the last term

$$a_{t-\Delta t \rightarrow t} = \frac{a(t) + a(t-\Delta t)}{2} \qquad \text{Eq. 2.12}$$

corresponds to the average acceleration between $t - \Delta t$ to t. Another expression for the average acceleration between $t - \Delta t$ to t is given by

$$a_{t-\Delta t \rightarrow t} = \frac{\Delta v}{\Delta t} = \frac{v(t) - v(t-\Delta t)}{\Delta t} \qquad \text{Eq. 2.13}$$

This equation along with the equation for position time t,

$$y(t) = y(t-\Delta t) + v_{t-\Delta t \rightarrow t}\Delta t + \frac{1}{2}a_{t-\Delta t \rightarrow t}\Delta t^2 \qquad \text{Eq. 2.14}$$

can be replaced into Eq. 2.11, which in turn can be solved for the blade's speed $v(t)$, as follows

$$v(t) = \frac{1}{C_1}\left[f_m(t) + f_m(t-\Delta t) + C_2 v(t-\Delta t) + 2ky(t-\Delta t) \right], \qquad \text{Eq. 2.15}$$

where

$$C_1 = k\frac{\Delta t}{2} + b + \frac{2m}{\Delta t} \qquad C_2 = \frac{2m}{\Delta t} - b \qquad \text{Eq. 2.16}$$

In the $v(t)$ expression (see Eq. 2.15) the magnetic force depends on the current *i(t)* and the blade position *y(t)* at the present time step *t*, therefore, Eq. 2.15 can be rewritten as

$$v(t) = \frac{1}{C_1}\left[f_m\left(y(t), i(t)\right) + f_m\left(t-\Delta t\right) + C_2 v\left(t-\Delta t\right) + 2ky\left(t-\Delta t\right) \right], \qquad \text{Eq. 2.17}$$

The electromagnetic system under study is finally described by a system of three equations: an equation for the current Eq. 2.7, and equation for the blade speed Eq. 2.15 and an equation for the blade position Eq. 2.14. The numerical solution to the system of equations described above can be found by repeatedly applying these equations, while reading from the lookup tables the values for inductance $L(y,i)$ and magnetic force $f_m(y,i)$.

Note that the coil's resistance has been deliberately excluded from the equations. It is an element that can easily be represented as an external component in the PSCAD/EMTDC program.

2.3 Finite element simulation

The solution to Eq. 2.7 and Eq. 2.15 requires the inductance and force to be known as functions of position and current. For such purpose a series of individual magneto-static FEA were performed for different air-gap openings as well as for different winding currents. As result, two three-dimensional matrices were obtained, one for the inductance $\mathbf{L}(y,i)$ and another one for the force $\mathbf{F}(y,i)$ [1]. These matrices, when fed to the PSCAD model described in Section 2.2, allow for the simulation of time dependant events. The next chapter provides a detailed description of the physical layout of the contactor modeled using this technique. It also presents the results obtained when comparing the decoupled method with transient FEA in terms of accuracy and in terms of simulation times.

---

[1] The measurement of the magnetizing force on the blade in the finite element simulation is calculated using the virtual work method [4] [5]. According to this method, the magnetic force on a magnetic material surrounded by air is given by

$$f_m = \frac{B^2 S}{2\mu_0}$$

where B is the flux density normal to the surface under consideration. In this case B corresponds to the $\vec{a}_y$ component of B in the air-gap.

3 CASE STUDY WITH THE NEW COMBINED APPROACH

This chapter evaluates the FEA-ETSP decoupled approach introduced in the precedent chapter in terms of computational speed and accuracy. For such purpose, the results of a series of simulations are compared against similar transient finite element simulations.

The error introduced in the decoupled approach by not modeling some stray inductive effects, namely eddy currents, is also studied.

3.1 PSCAD simulation setup

The inductance and force models $\mathbf{L}(y,i)$ and $\mathbf{F}(y,i)$ described in the previous chapter were found for a sample case and then incorporated as look up tables in the PSCAD model (see Figure 3-1). This PSCAD[2] model was in turn used to simulate the transient response of the contactor. Figure 3-2 details the circuit setup used in PSCAD. The upper part of this diagram accounts for the circuit given in Figure 2-2. Here, a gate turn-off thyristor GTO was used as the switching device. The two elements at the bottom of the

---

[2] The PSCAD simulation uses linear interpolation when reading $\mathbf{L}(y,i)$ and $\mathbf{F}(y,i)$ matrices.

diagram represent the modules in charge of reading the lookup models for inductance $\mathbf{L}(y,i)$ and magnetic force $\mathbf{F}(y,i)$.

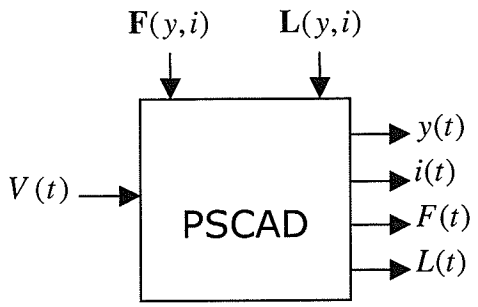

Figure 3-1 PSCAD contactor general layout

3.2 2D FE setup

The FE two-dimensional representation of the contactor was obtained by taking a vertical slice through the contactor with the core laminations stacked normal into the page. The model contained the two sides of the coil and assumed it extends normal to the plane shown a length *d*. A.B.J. Reece *et al* [1] suggests that when using 2D finite element solvers to represent 3D problems, the length normal to the simulation plane used should be such that it gives the same core cross-sectional area as the real three dimensional geometry. In this case, since the core section was rectangular, the length taken (1 cm) is the same as the *real* geometry of the device.

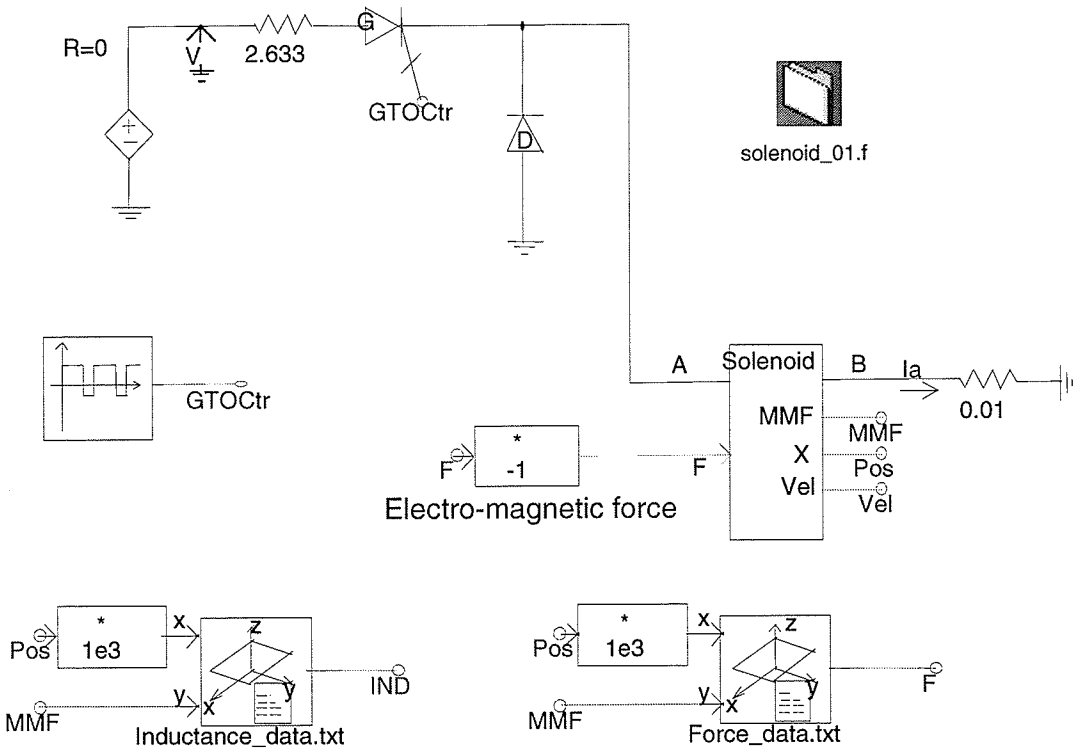

Figure 3-2 PSCAD contactor circuit simulation layout

3.3 Contactor's physical layout

The dimensions of the contactor studied are given in Figure 3-3. The depth of the contactor was 1 cm.

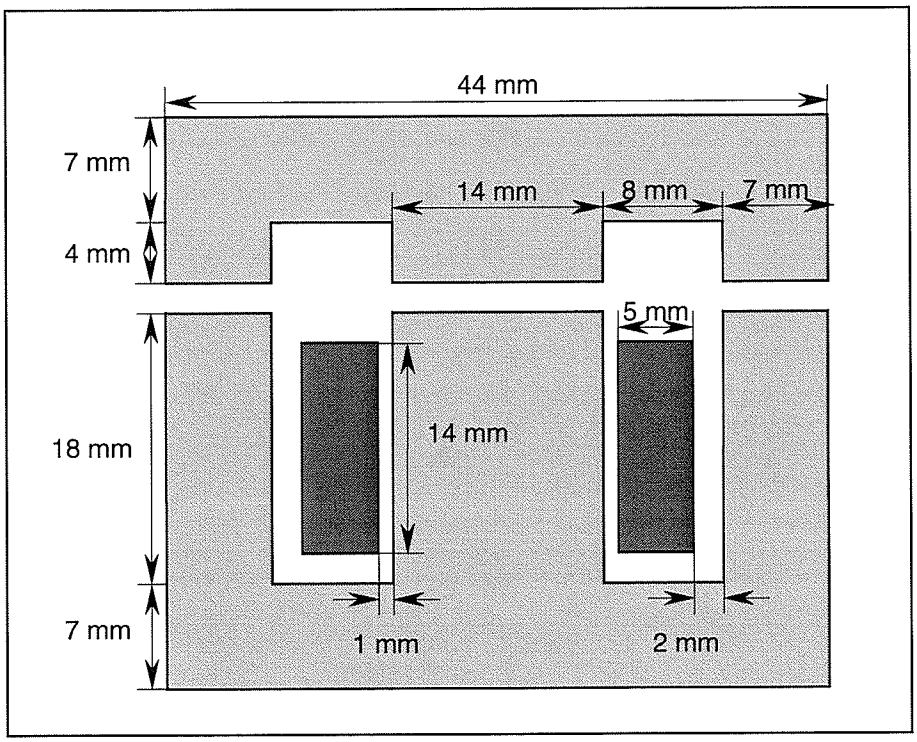

Figure 3-3 Contactor dimensions

The values of some of the construction and electrical parameters were:

$m = 32.09$ g	mass of blade
$k = 1000$ N/m	spring constant
$N = 250$	number of turns in the coil
$r_C = 2.368\ \Omega$	coil resistance
$r_S = 2.633\ \Omega$	Series resistance (see Figure 2-2)
$y_{max} = 8$ mm	maximum opening of the air gap

$y_0 = 6$ mm — air gap at rest

$V = 25$ Vdc — source voltage

$b = 6$ N.s/m — friction coefficient

$\rho_0 = 1\ \Omega$.m — resistivity of core material

In order to simplify the analysis, the core material was assumed to be magnetic steel with ***isotropic*** non-linear permeability. The steel saturation was defined using one of the equations proposed in the Flux 2D/3D documentation [3] (see Eq. 3.1). Figure 3-4 plots the magnetic flux B versus the magnetic field intensity H for the chosen parameter values.

$$B(H) = \mu_0 H + B_S \frac{H_a + 1 - \sqrt{(H_a+1)^2 - 4H_a(1-a)}}{2(1-a)} \qquad \text{Eq. 3.1}$$

where:

$$H_a = \mu_0 H \frac{\mu_r - 1}{J_S}$$

$B_S = 1.9$ T — saturated flux density

$\mu_r = 1000$ — linear relative permeability (slope at the beginning of the curve)

a = 0.3 bend adjustment coefficient

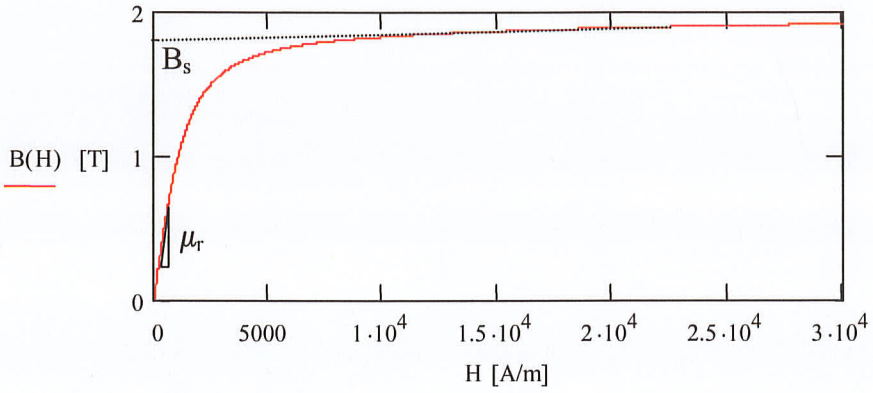

Figure 3-4 B-H curve of the contactor core material

3.4 Results

As was previously described in Section 1.1.2, transient magnetic simulations are time stepped FEA coupled with ETSP. This type of analysis was used as reference point to evaluate the error introduced in the PSCAD simulation by: i) the level of discretization on the $\mathbf{L}(y,i)$ and $\mathbf{F}(y,i)$ matrices and, ii) by neglecting some time dependent phenomena such as eddy currents. For this purpose, a series of tests were performed where the same voltage wave shapes $V(t)$ used to excite the PSCAD model were used to excite the transient magnetic finite element engine FEA(t) while measuring the same set of parameters: position, force on the blade, current and inductance Figure 3-5.

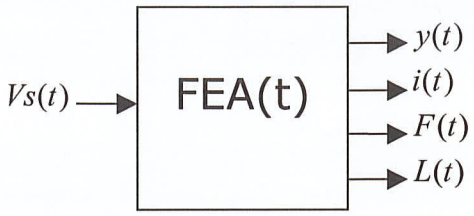

Figure 3-5 Transient magnetic FEA

3.4.1 Discretization level

The inductance $\mathbf{L}(y,i)$ and force $\mathbf{F}(y,i)$ models are depicted in Figure 3-7. The blade was assigned a movement range of 8 mm sampled in 32 equal intervals of 0.25 mm, and the coil ampere-turns were assumed could take values from zero up to 1300 A, sampled in 52 equal intervals of 25 A. This made for a total of 1749 FEA which took 48.4 minutes of processing time. The computer used was a PC with a 3 GHz Pentium 4 processor and 1.0 GB of RAM. The contactor was modeled using 8675 nodes and 3912 surface elements.

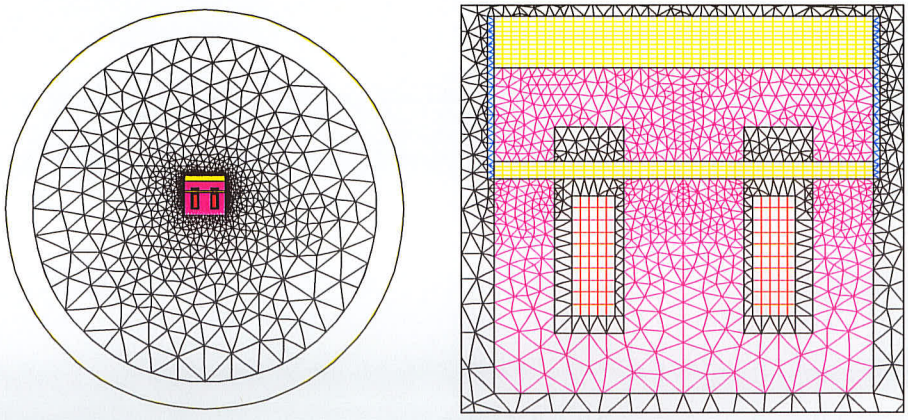

Figure 3-6 a) Contactor finite element layout. b) Zoom of the contactor

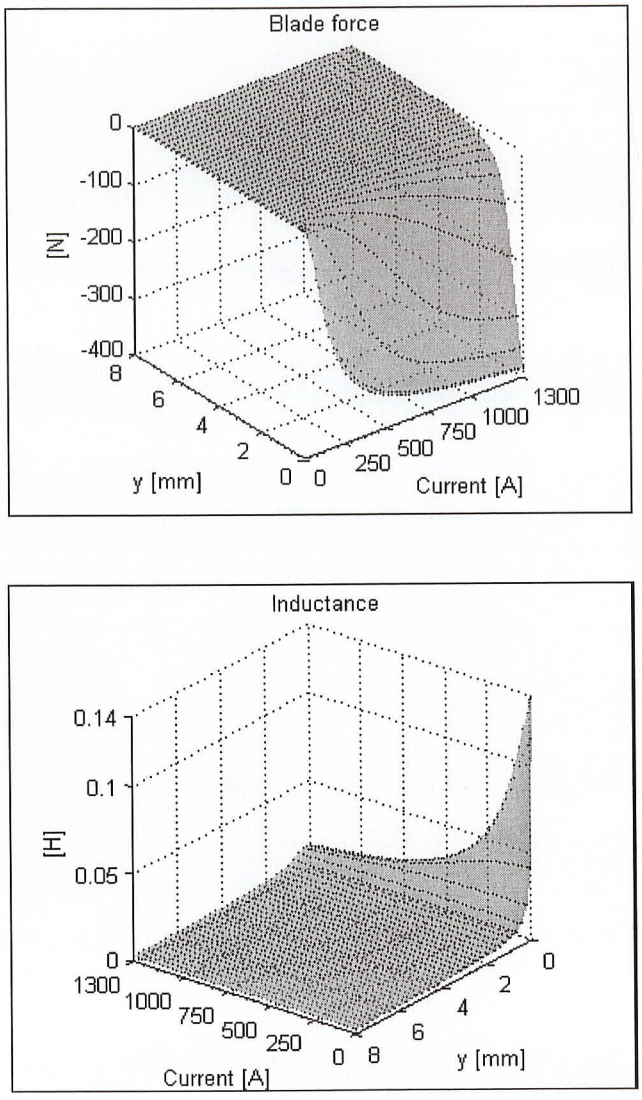

Figure 3-7 Blade force $\mathbf{F}(y,i)$ and inductance $\mathbf{L}(y,i)$ models

In the first test, the contactor winding was connected to a voltage source and excited with a pulse (see Figure 3-8). The results for ampere-turns, magnetic force, and blade position inductance as a functions of time obtained with both, PSCAD and Transient-magnetic FEA are shown in Figure 3-9.

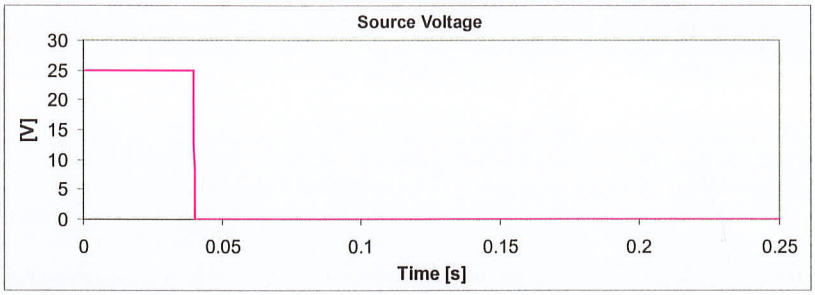

Figure 3-8 Source voltage

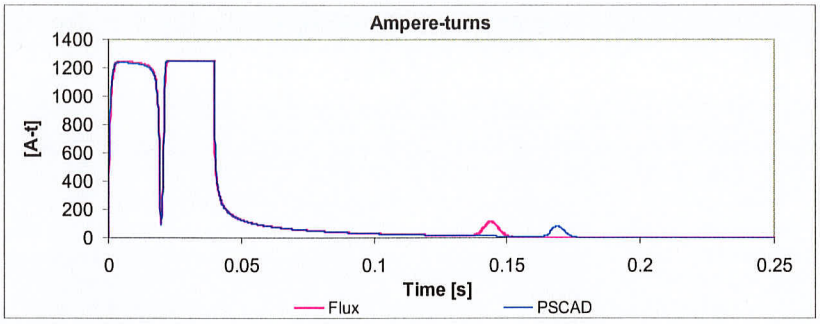

a)

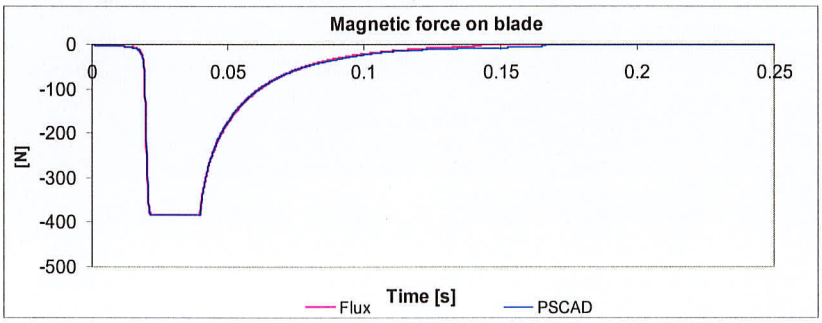

b)

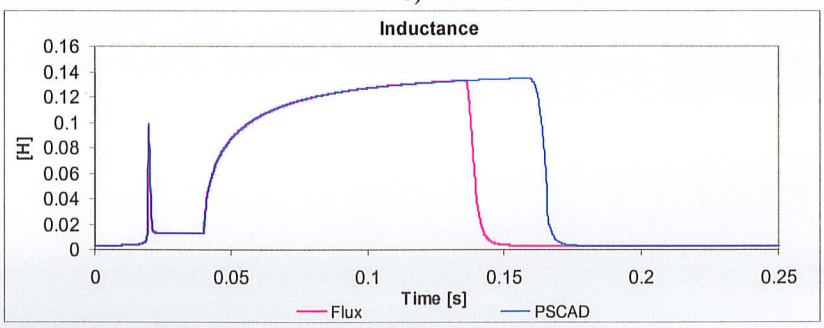

c)

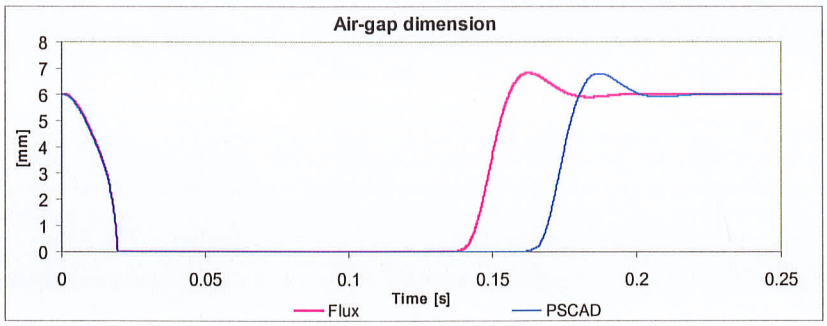

d)

Figure 3-9 Base case: comparison between transient magnetic FEA and PSCAD simulations for a) winding ampere turns, b) magnetic force on blade, c) coil inductance and d) air-gap dimension y

These plots present high similitude in wave shapes between the two different methods, however with a discrepancy in the time at which the air-gap starts reopening (see Figure 3-9.-d). The contactor in the transient FEA simulation opens earlier than in the FEA-ETSP simulation.

Taking a closer look at Figure 3-7, it can be seen that the non-linearity of $\mathbf{F}(y,i)$ and $\mathbf{L}(y,i)$ is highly pronounced at very small air-gaps. Therefore, it could be expected for the PSCAD model to be more inaccurate in this region.

An improvement in the transient performance of the PSCAD model was achieved by refining the grid of the $\mathbf{F}(y,i)$ and $\mathbf{L}(y,i)$ models on the most non-linear regions. For this reason, new magneto-static FEA were run for

y=[0.001 0.1 0.5 0.1 0.15 0.2 0.25 0.3] mm

i=[0.004 0.02 0.04 0.08 0.1 0.12] A

The results for force and inductance where inserted into the $\mathbf{F}(y,i)$ and $\mathbf{L}(y,i)$ models. Figure 3-10 re-plots Figure 3-9 for the new air-gap and current sampling. It can be seen that the error in the PSCAD transient simulation diminished considerably. All the curves, decoupled FEA-ETSP and transient FEA match almost perfectly when superimposed.

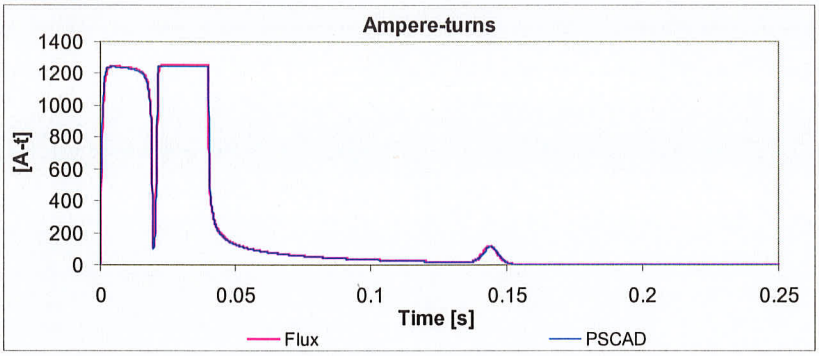

a)

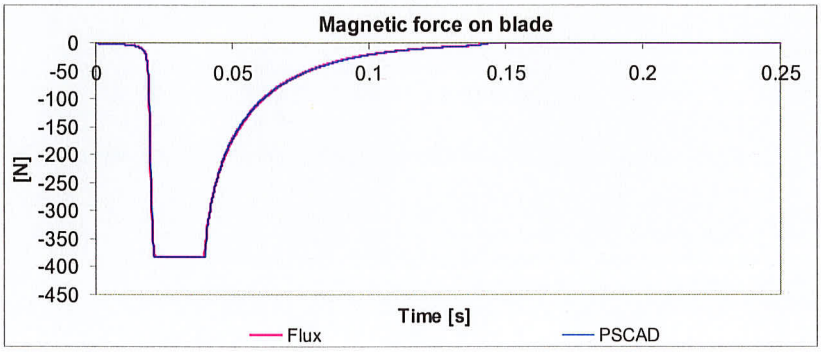

b)

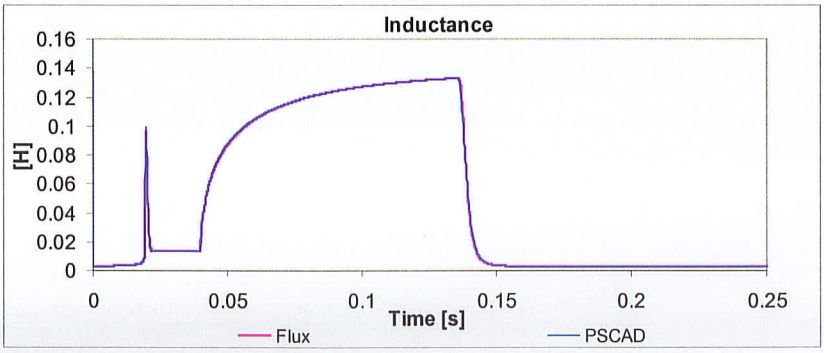

c)

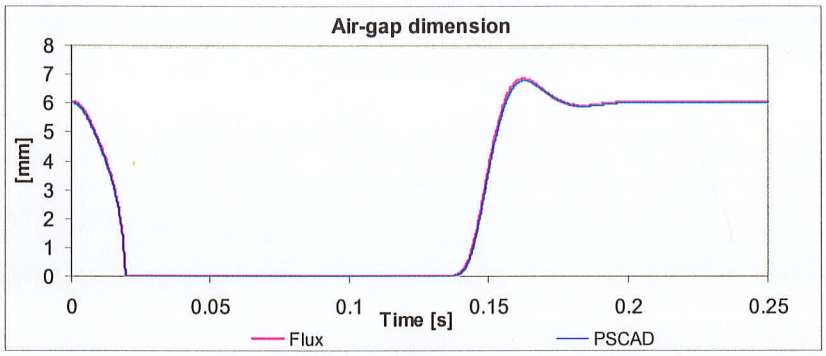

d)

Figure 3-10 Transient magnetic FEA - PSCAD comparison with improved sampling. a) Winding ampere turns b) magnetic force on blade c) coil inductance and d) air-gap dimension *y*

3.4.2 Simulation times

The main purpose of the technique introduced in the previous and present chapters was to provide a high speed, yet accurate, method for simulating transients in electromagnetic systems that contain non-linear components. So far it has proven to be accurate. Table 3-1 presents the computation times used by the transient FEA and the decoupled FEA-ETSP methods. It can be observed that as expected, the decoupled method was considerably faster by approximately 520 times.

Simulation method	**Time**
Transient magnetic FEA	1h 31s
PSCAD	7s
Preprocessing FEA time	67 min (*)

Table 3-1 FEA and PSCAD computation times (*) Includes added magnetostatic FEA for improved discretization (see previous section)

It should be noted that to ensure comparability, both simulations, transient FEA and PSCAD, used the same time step Δt of 200 μs.

3.4.3 Electromagnetic induction effects

So far, the PSCAD model has provided a fast and excellent representation of the electro-mechanical device under study. However, as currently formulated, it does not take into account certain time dependant electromagnetic effects such as eddy currents and displacement currents. When these effects are considered, the quasi-static manner in which $\mathbf{F}(y,i)$ and $\mathbf{L}(y,i)$ were derived is not completely accurate.

In the typo of electromagnetic system under study, displacement currents can essentially be seen as capacitive currents. There are two main kinds of capacitance in the contactor arrangement, winding stray capacitance (turn to turn capacitance) and winding to ground capacitance. In order to simulate winding stray capacitance in FEA, every turn in the winding would have to be individually represented. This would have been very labour and computing time intensive. For simplicity, in this paper the coils were represented in macro scale as single pieces of solid conductor carrying the total ampere-turns. This simplification eliminated the possibility of analyzing the effects of winding eddy currents and winding stray capacitance.

As is well known in the power transformer industry, the effects of winding to ground and turn to turn capacitance become significant only when dealing with high frequencies (MHz). Hence for the purpose of this thesis displacement currents could be neglected.

With this, the only time dependant phenomena whose impact could be analyzed was the effect of eddy currents in the core.

Originally, the core resistivity was chosen to be ρ_0 = 1 Ω.m. In this case, the induced eddy currents in the core did not play a key roll since their measured densities were very small, less than 6.7μA/m^2 at its maximum.

In order to enhance the effect of core eddy currents, a new case, somewhat extreme and unrealistic, was run assuming a solid core (no laminations) with a resistivity of ρ_0 = 0.16 μΩ.m. In this new simulation, an appreciable difference in the system response was observed between the transient FEA and the PSCAD simulations, see Figure 3-11. The current in the FE simulation decreased slightly faster than in the PSCAD model, which translated into a faster re-opening of the contacts. In this case, the density of the core eddy currents reached a peak value of 2.1 A/m^2.

A method that could be used to account for the faster damping of the current is the introduction of damping resistors; however its implementation goes beyond the scope of this thesis.

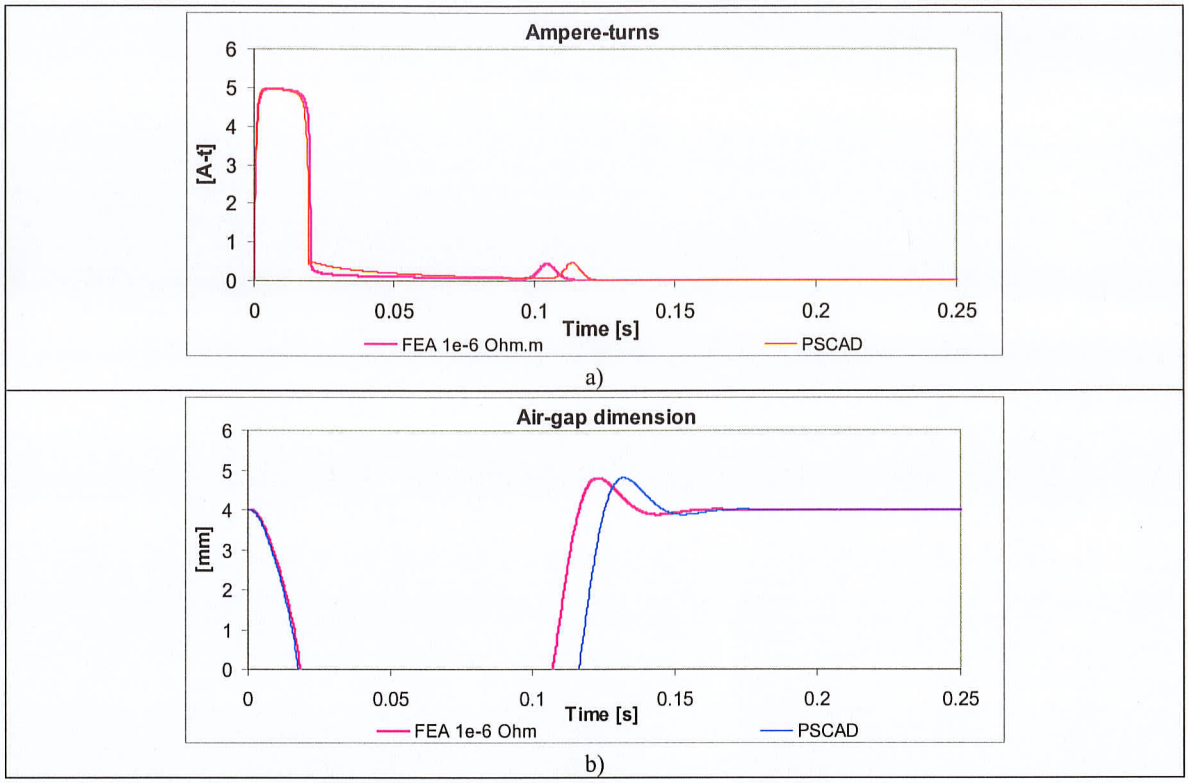

Figure 3-11 Transient magnetic FEA for different core resistivities. a) Winding ampere turns, b) air-gap dimension y

3.4.4 Trapezoidal wave

In order to see how well the FEA-ETSP decoupled method worked with time varying excitation, the contactor was excited with a trapezoidal voltage wave instead of the dc voltage used earlier (see Figure 3-12). The transient magnetic FEA simulation used to evaluate the accuracy of the decoupled FEA-ETSP method was run using a core resistivity of 1.0 Ωm. The results of this simulation are shown in Figure 3-13. It can be seen again that there is hardly any difference between the more accurate transient FE and the simplified decoupled FEA-PSCAD simulations.

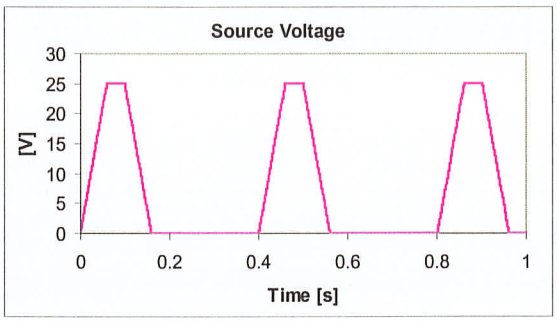

Figure 3-12 Trapezoidal voltage source

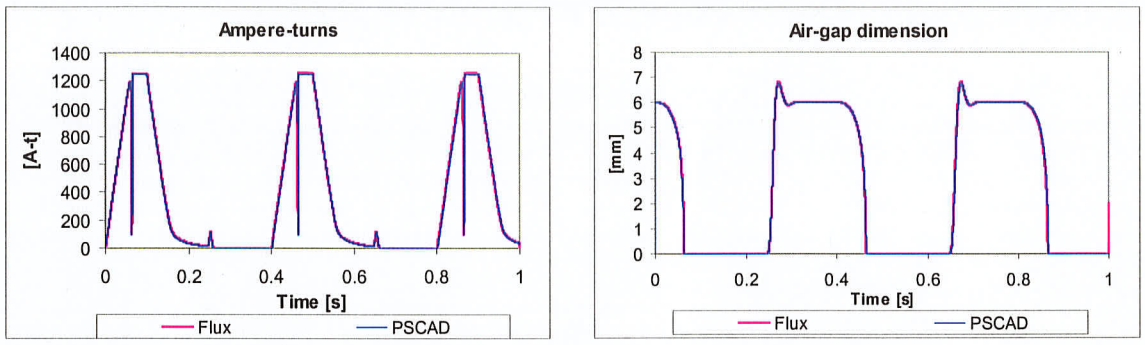

a) b)

Figure 3-13 Transient magnetic FEA - PSCAD comparison for a trapezoidal voltage source. a) Winding ampere turns, b) air-gap dimension *y*

So far the use of FEA and ETSP in a decoupled manner has proven to be remarkably accurate for simulating transient events in a single non-linear inductor electromagnetic system. This conclusion is valid as long as the eddy currents do not play a key role in the system performance.

The next chapter explores the performance of the decoupled method on an electromagnetic system with a higher degree of complexity that involves the modeling of non-linear mutual inductances.

4 MODELING OF A SINGLE-PHASE TWO-CIRCUIT TRANSFORMER BY THE LOOK-UP METHOD

This chapter has the purpose of evaluating the performance of the decoupled FEA-ETSP method introduced in the previous chapters in a more complex electromagnetic system. For this reason a two-winding single-phase transformer was chosen. This new system provides the opportunity of assessing the method's performance at simulating mutual non-linear impedances.

A simple representation of the transformer under study is provided on Figure 4-1. Here the magnetic paths are represented with dotted lines for the main flux ϕ_1, and solid lines for leakage fluxes $\phi_{\sigma 1}$ and $\phi_{\sigma 2}$.

4.1 ETSP modeling

The transformer general voltage equations written in terms of the windings' flux linkages are given by

$$v_1 = i_1 r_1 + n_1 \frac{d}{dt}[\phi_1 + \phi_{\sigma 1}] \qquad \text{Eq. 4.1}$$

$$v_2 = i_2 r_2 + n_2 \frac{d}{dt}[\phi_1 + \phi_{\sigma 2}]$$

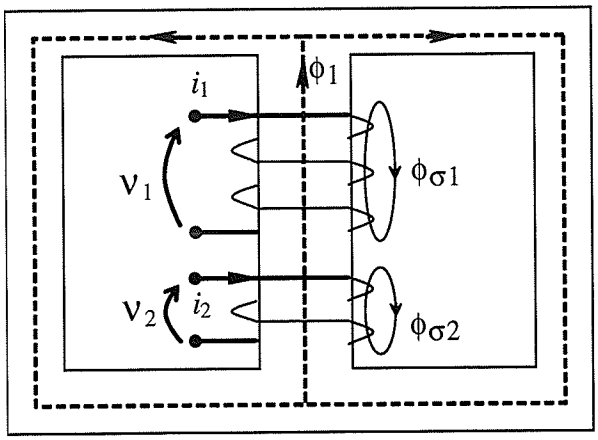

Figure 4-1 Voltages, currents and fluxes in the single-phase transformer

where r_i are the winding's ohmic resistances and n_i the number of turns in winding i.

These equations can be rewritten in terms of variable inductances as follows

$$\begin{bmatrix} v_1 \\ v_2 \end{bmatrix} = \begin{bmatrix} r_1 & 0 \\ 0 & r_2 \end{bmatrix} \begin{bmatrix} i_1 \\ i_2 \end{bmatrix} + \frac{d}{dt} \left\{ \begin{bmatrix} L_{11} & L_{12} \\ L_{12} & L_{22} \end{bmatrix} \begin{bmatrix} i_1 \\ i_2 \end{bmatrix} \right\} \qquad \text{Eq. 4.2}$$

where L_{11} and L_{22} are the winding's self inductances and L_{12} and L_{21} the mutual inductances.

Eq. 4.2 can be rewritten in matrix form as

$$\mathbf{V}(t) = \mathbf{r}\,\mathbf{i}(t) + \frac{d}{dt}\left[\mathbf{L}(t)\mathbf{i}(t)\right] \qquad \text{Eq. 4.3}$$

The expression to be used in the ETSP was found by solving Eq. 4.3 for i(t) using the trapezoidal approach, i(t) is then given by

$$\mathbf{i}(t)=\left[\mathbf{r}\frac{\Delta t}{2}+\mathbf{L}(t)\right]^{-1}\left\{\left[\mathbf{V}(t)+\mathbf{V}(t-\Delta t)\right]\frac{\Delta t}{2}+\left[\mathbf{L}(t-\Delta t)-\mathbf{r}\frac{\Delta t}{2}\right]\mathbf{i}(t-\Delta t)\right\} \quad \text{Eq. 4.4}$$

4.2 The look-up model

Similar to the approach in Chapter 3, the use of Eq. 4.3 as part of the ETSP decoupled simulation method requires the construction of a mapped model of the self L_{ii} and mutual inductances $L_{ij}\big|_{i\neq j}$.

The challenge in constructing such models arises in the need for knowing how much of the flux linking a given winding is product of the current flowing through the winding itself and how much is due to the current circulating through the neighboring windings. In order to overcome this difficulty it was necessary to make a couple of assumptions. The first one was that given the material's B-H curve, the inductance maximum value occurs when the magnitude of the transformers net magneto-motive force is at its minimum (see Eq. 4.5). This is valid since the inductance is directly proportional to the material magnetic permeability μ, where μ is the slope in the B-H curve (see Figure 4-6). In the approximated B-H curve used here to represent the material, the maximum slope occurs at low values of magnetic field intensity H. Where, H happens to be directly proportional to the net magneto-motive force *mmf* across the material. It is therefore reasonable to assume that inductance maximum value occurs at the point where the *mmf*'s magnitude is at its minimum.

$$mmf = n_1 i_1 - n_2 i_2 \qquad \text{Eq. 4.5}$$

Figure 4-2 exemplifies the general shapes for the net mmf, winding 1 inductance and flux linkage λ_1 in function of i_1 for a constant value of i_2.

The second assumption, exemplified in terms of winding 1 self inductance, was that the mutual inductance L_{12} remains unchanged for small changes of i_1 for as long as i_2 is kept constant.

With these assumptions a method for measuring L_{11} was developed as explained in the following paragraphs.

As starting point, winding 1 flux linkage vs. current curve in Figure 4-2 was chosen to be redrawn as $\lambda_1 - L_{12} i_2$ for easier analysis (see Figure 4-3). This curve was in turn modeled in terms or several segments, where a given k^{th} segment was delimited by two different values of measured flux linkage $\lambda_1^{k-1} - L_{12} i_2$, $\lambda_1^{k} - L_{12} i_2$ and current i_1^{k-1}, i_1^{k}.

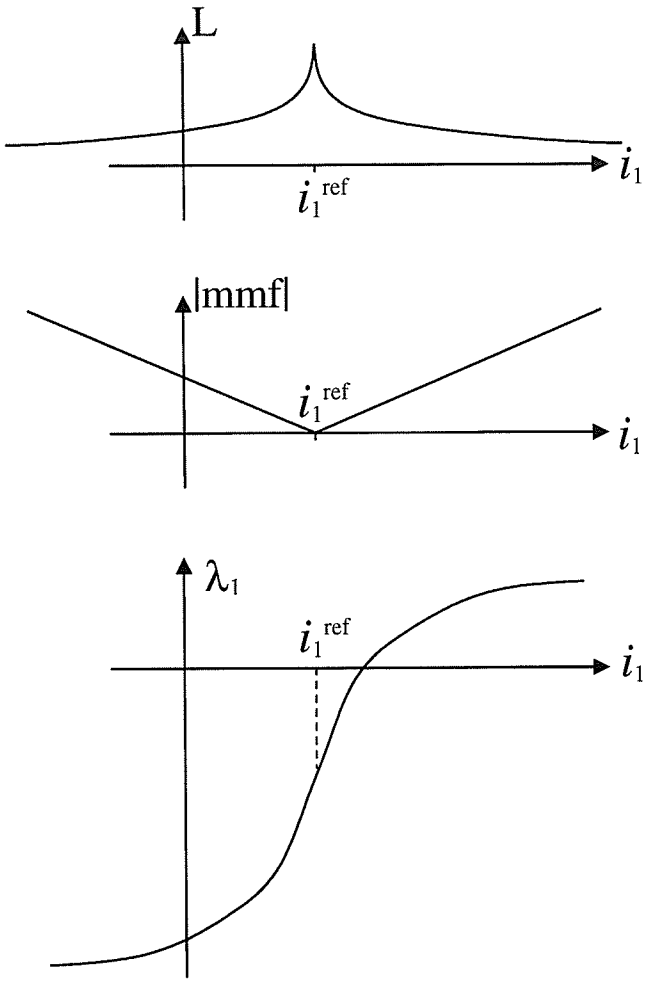

Figure 4-2 General shape of inductance L, magneto-motive force mmf and flux linkage vs. winding 1 current for a constant value of winding 2 current

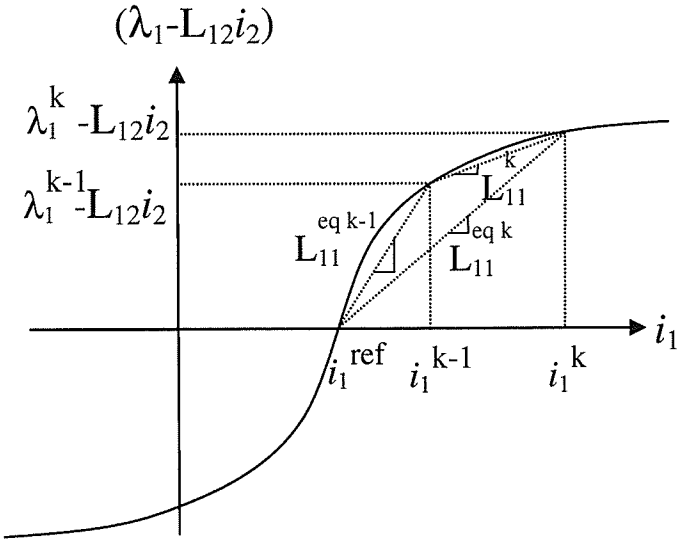

Figure 4-3 Inductance model using linear splines

From Figure 4-3 an expression for the flux linkage $\lambda_1 - L_{12} i_2$ at k-1 and k can be written as

$$\lambda_1^{k-1} - L_{12} i_2 \approx L_{11}^{eq\,k-1} i_1^{k-1} \qquad \text{Eq. 4.6}$$

$$\lambda_1^{k} - L_{12} i_2 \approx L_{11}^{eq\,k-1} \left(i_1^{k-1} - i_1^{ref} \right) + L_{11}^{k} \left(i_1^{k} - i_1^{k-1} \right)$$

An equivalent inductance L_{11} at k such that

$$\lambda_1^{k} - L_{12} i_2 \approx L_{11}^{eq\,k} \left(i_1^{k} - i_1^{ref} \right) \qquad \text{Eq. 4.7}$$

can be found by combining Eq. 4.6 and Eq. 4.7 and solving for $L_{11}^{eq\,k}$, as follows

$$L_{11}^{eq\,k} \approx \frac{L_{11}^{eq\,k-1}\left(i_1^{k-1} - i_1^{ref}\right) + L_{11}^{k}\left(i_1^{k} - i_1^{k-1}\right)}{i_1^{k} - i_1^{ref}} \qquad \text{Eq. 4.8}$$

where i_1^{ref} is given by

$$i_1^{ref} = \frac{n_2}{n_1} i_2\Big|_{CONSTANT} \qquad \text{Eq. 4.9}$$

This $L_{11}^{eq\,k}$ equation provides the inductance to be used when $i^{k-1} \le i < i^{k}$ for a given value of i_2

A similar expression can be found for L_{21} keeping i_2 constant and varying i_1. Expressions for L_{12} and L_{22} can be found by keeping i_1 constant and varying i_2. Table 4-1 summarizes the procedure used to measure the transformer's impedance matrix.

Calculate	Measure	Constant	Variable
L_{11}	λ_1	i_2	i_1
L_{12}	λ_1	i_1	i_2
L_{21}	λ_2	i_2	i_1
L_{22}	λ_2	i_1	i_2

Table 4-1 Measurement of the two-winding single-phase transformer impedance matrix

4.3 FE simulation

The transformer's transient FE simulation was setup using an axi-symmetric engine. For this purpose the core was unfolded and represented as a straight section of length Lc,

where this length corresponds to the effective length of the single phase transformer core (length of core legs plus core yokes).

One of the requirements imposed by the FE software used is that in order to read the flux linked by any given winding, the geometry under study must include the full path or complete cycle of the magnetic lines. For this purpose, the flux lines path was closed by introducing a return path. This return path had to be designed such that its reluctance should be depreciable when compared with the reluctance of the core (*Lc* section). For such purpose the permeability chosen for the return region (shown in dark color in Figure 4-4) had to be very high. A relative permeability $\mu_r = 1x10^6$ was chosen for this region.

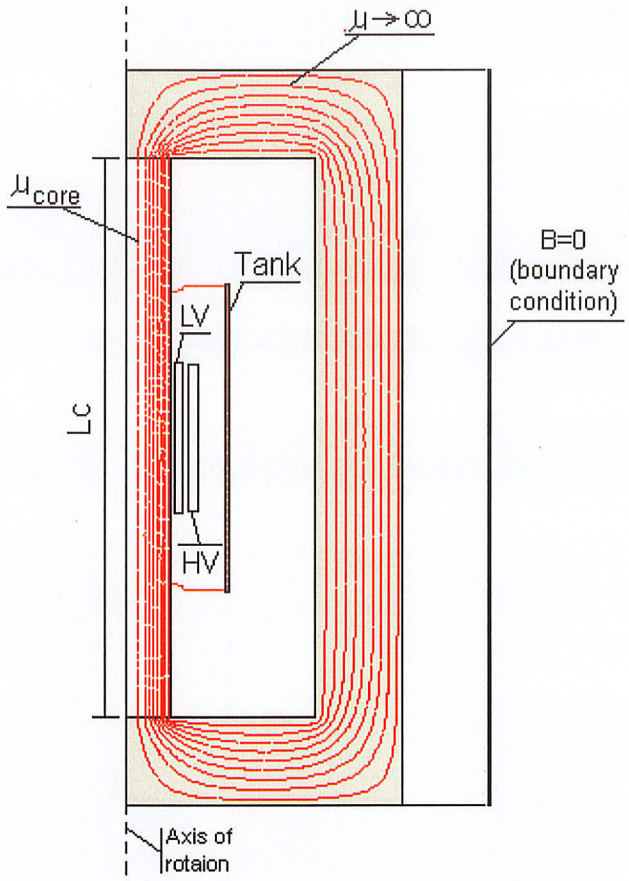

Figure 4-4 Axi-symmetric representation of single-phase transformer

The dimensions of the transformer studied are given in Figure 4-5. As well, the values of some of the construction and electrical parameters are

S = 15 MVA	transformer's rated power
n_1 = 40	number of turns in secondary coil (LV)
n_2 = 133	number of turns in primary coil (HV)
r_1 = 20 mΩ	secondary winding resistance

$r_2 = 0.5\ \Omega$	primary winding resistance
$A = 0.441\ m^2$	area of transformer main core leg
$V_1 = 7967$ V RMS	low voltage winding nominal line to ground voltage
$V_2 = 26558$ V RMS	high voltage winding nominal line to ground voltage
Bn = 1.696 T	nominal core flux density at 60 Hz
Lc = 6.75 m	total equivalent length of core (see Figure 4-4)

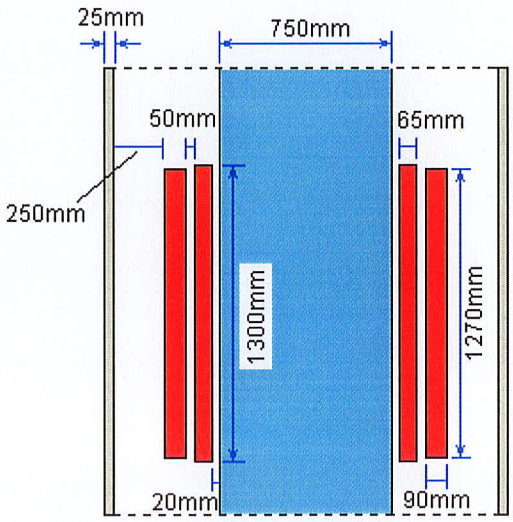

Figure 4-5 General layout of single-phase transformer under study

The core material was assumed isotropic with B-H curve described by Eq. 3.1. The parameters chosen were B_S=2.06T, μ_r=75000 and a=0.5. Figure 4-6 displays the new B-H curve.

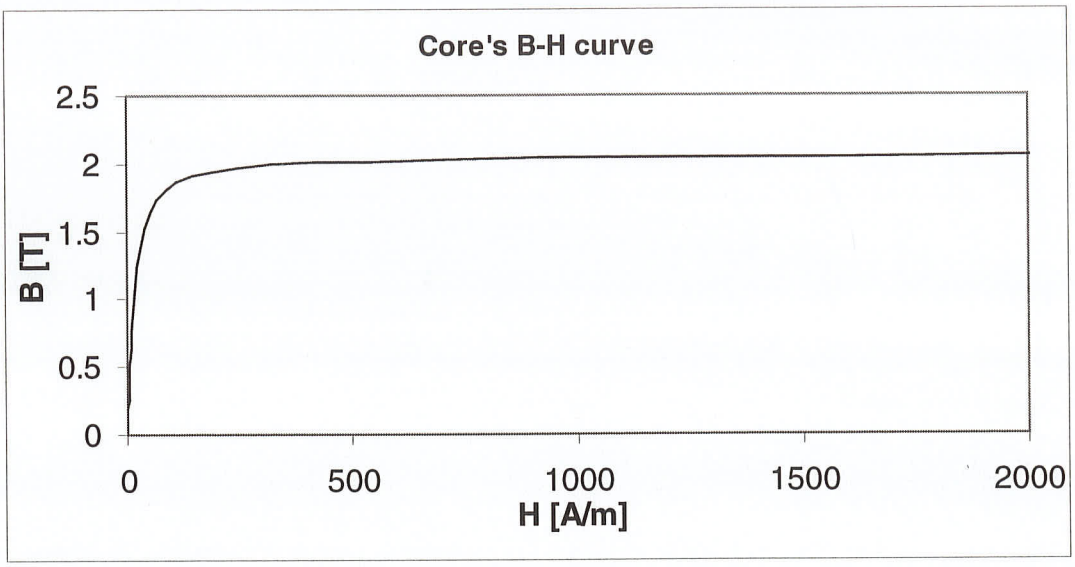

Figure 4-6 Core's B-H curve

4.3.1 Inductance models

The L_{11} and L_{21} inductance models were built by running multiple magneto-static FE simulations. Detailed sampling was carried out around the regions where the non-linearity was found to be more pronounced, and fewer samples in the region where the core magnetic material starts to behave linearly pass the saturation point.

Figure 4-7 and Figure 4-8 show the inductance model for L_{11} and L_{21}. Please note that in all cases one of the axes was normalized. This was done for convenience reasons, since it made writing the ETSP code easier.

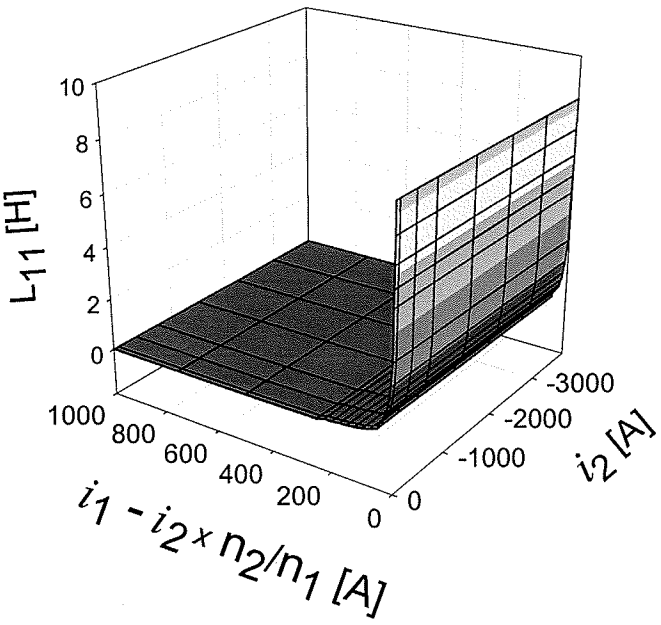

Figure 4-7 Inductance lookup model: L_{11}

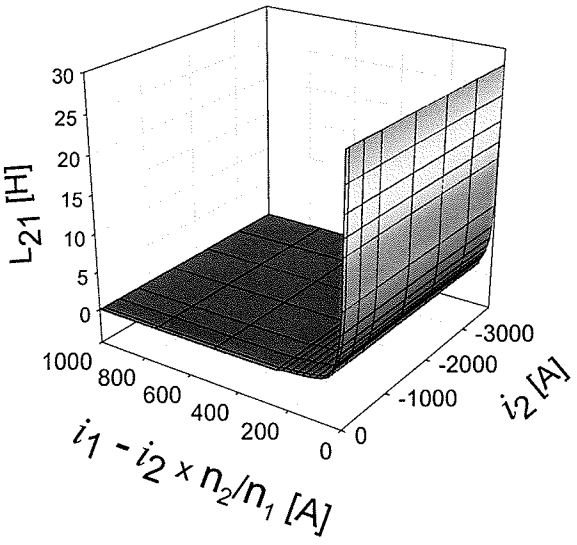

Figure 4-8 Inductance lookup model: L_{21}

Similar diagrams were obtained for L_{12} and L_{22}

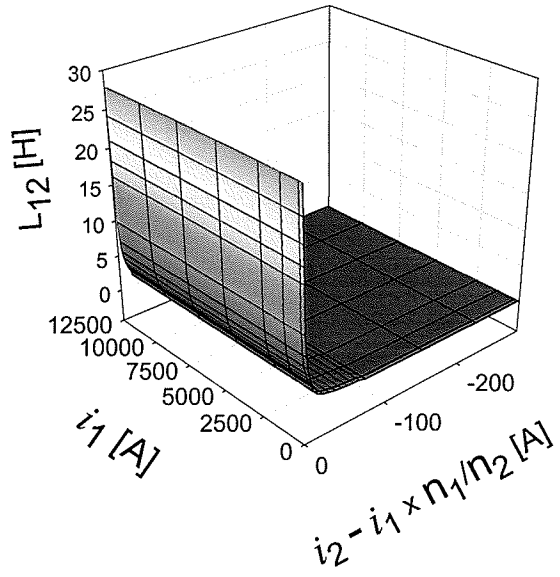

Figure 4-9 Inductance lookup model: L_{12}

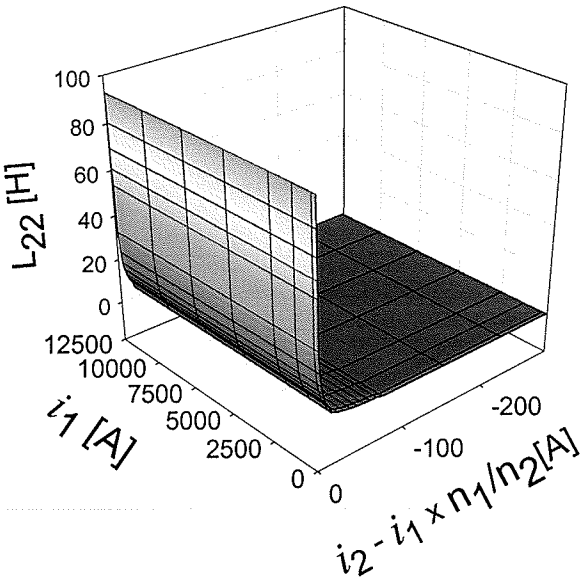

Figure 4-10 Inductance lookup model: L_{22}

4.4 Simulation results

Two different cases were simulated using the FEA-ETSP decoupled model and compared against similar transient FEA. Each one of these cases, as it will be explained, was designed to test different aspects of the decoupled model.

4.4.1 Impedance voltage

In the first test, the transformer's impedance voltage IeX% was measured. Where IeX% is, in percentage of the nominal voltage, the voltage that when applied to the transformer's primary circuit, produces nominal current to flow while having the secondary shorted. The difference between the voltage measured using the look-up model and transient FEA was found to be minute (see table below).

	FEM	Look-up method	Difference
IeX%	4.36	4.29	1.61%

Table 4-2 Transformer impedance voltage calculation with transient FEA and look-up method

This test was intended to evaluate the leakage inductance modeling.

4.4.2 Cold energization

This is an inrush-like simulation where the transformer is switched on without having any remanent flux in the core. In this particular test the secondary winding was left open.

Figure 4-11 shows that the difference between the transient FEA and the look-up simulations is minimum, where the difference for the first peak was of 7.9%.

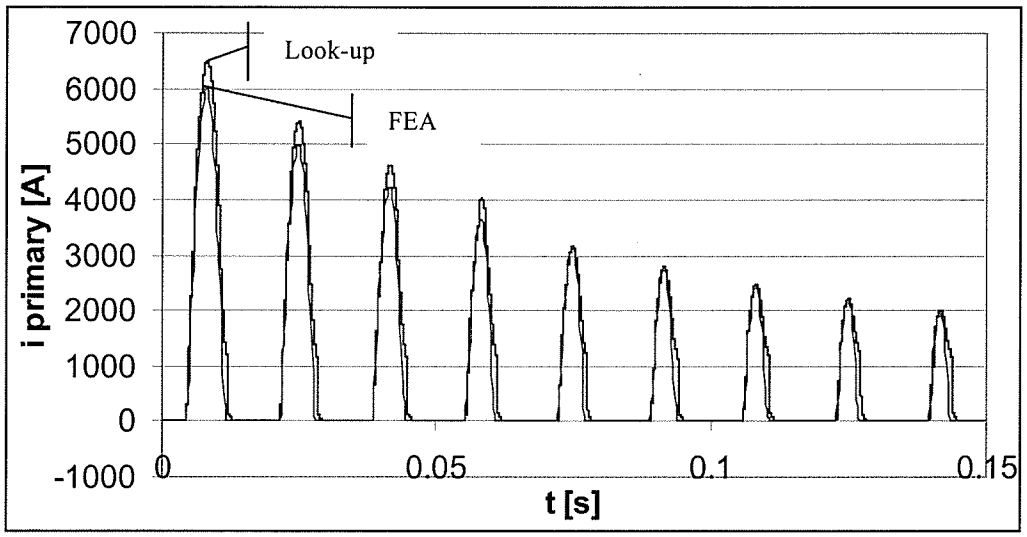

Figure 4-11 Transformer energization with 26558 V RMS (1.0 p.u. voltage)

This test was intended to drive the transformer into saturation. However, it does not test the transformer interaction between windings mutual inductances currents, since the secondary winding is open with zero current. Due to time limitations, the candidate could not carry out a simulation that fully tests the interaction between windings. It is important for future works in this field to perform this test in order to validate the technique proposed here in full spectrum.

Both tests show that the FEA-ETSP decoupled method produces good results in the simulation of a geometry that involves two windings. Similarly to Chapter 3, considerable savings in simulation time were also achieved in this new electromagnetic

system. The transient FEA performed in the second test took 81 minutes while the look-up method took only 32 s of computation time.

The next chapter presents one of the biggest limitations of the decoupled method and provides and alternative simulation technique for highly complex electromagnetic systems.

5 THREE-PHASE THREE-CIRCUIT FIVE-LIMB CORE TYPE TRANSFORMER

This chapter discusses a more complicated electromagnetic system with several coils. In the preceding chapters the inductance models used in the contactor and two winding transformer transient electromagnetic models were built by running multiple independent FEA.

At first glance, it appears that inductance models of size nxn can be derived from multiple magnetostatic FEA. However, in the case of three-phase three-circuit transformers, the number of currents to be sampled would be nine, one for each winding. If a sampling level of 10 different values were selected for each of these variables, the number of magnetostatic FE runs necessary to construct the model would be 10^9. Written in terms of computing time, it would take 57 years[3] to map the model. This proves that

---

[3] The computing time was estimated assuming the same number of finite elements and computer setup used in the contactor arrangement.

this method is highly impractical for cases with several variables if not used in conjunction with an efficient learning algorithm.

In this chapter, unlike the previous chapters, the magnetic model of the electromagnetic system under study to be used as part of the ETSP is not built the product of a collection of magneto-static FEA. Instead, a well known method utilized in ETSPs is used. In this method, an equivalent lumped magnetic circuit is built based on the transformer's physical configuration (ignoring flux fringing effects). This magnetic circuit is in turn coupled with the transformer's equivalent lumped circuit.

The electrical circuit of the transformer was developed under the assumption that the leakage inductance remains constant over time. The magnetic circuit was built taking into account the non-linearity of the core material by means of linear splines. Once formulated, the equations that describe the magnetic-electric coupled system were solved numerically in terms of time increments following the trapezoidal approach. At the end of this chapter some comparisons are made between the performance of this model against a transient FE model for different levels of induction in the steady state.

5.1 Transformer lumped electrical circuit

Figure 5-1 presents a general scheme of the three-phase three-circuit five-limb transformer under study.

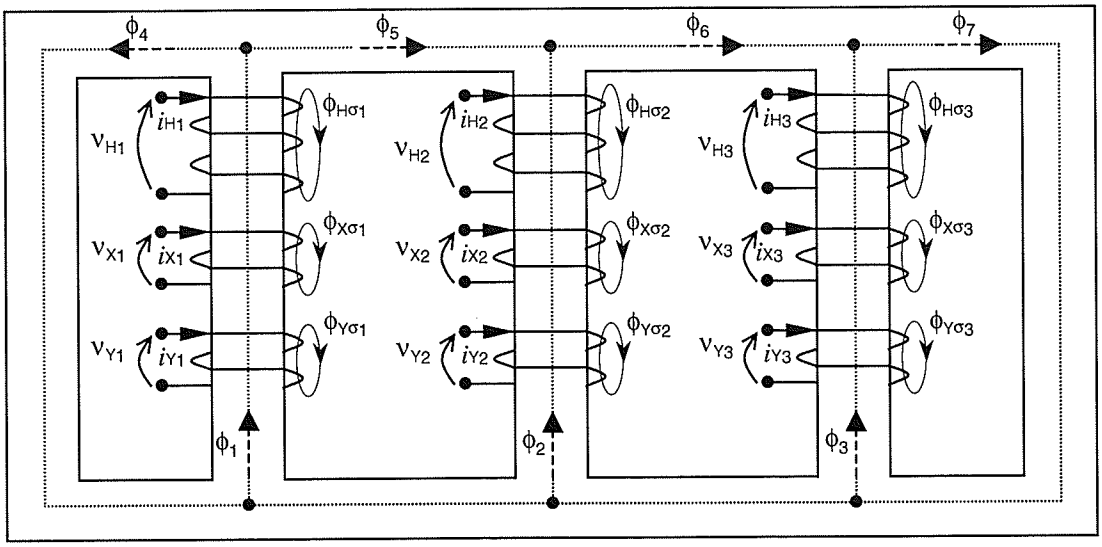

Figure 5-1 Voltages, currents and fluxes in the five-limb transformer

The voltage equations for the transformer in Figure 5-1 are given by

$$v_{Hi} = i_{Hi} r_{Hi} + n_H \frac{d}{dt}\left[\Phi_i + \Phi_{H\sigma i}\right]$$

$$v_{Xi} = i_{Xi} r_{Xi} + n_X \frac{d}{dt}\left[\Phi_i + \Phi_{X\sigma i}\right] \qquad \text{Eq. 5.1}$$

$$v_{Yi} = i_{Yi} r_{Yi} + n_Y \frac{d}{dt}\left[\Phi_i + \Phi_{Y\sigma i}\right]$$

where r_{Hi}, r_{Xi} and r_{Yi} are the ohmic resistances of the primary, secondary and tertiary windings. n_H, n_X and n_Y are the numbers of turns of the primary, secondary and tertiary windings.

There have been two main approaches regarding the method used to incorporate the leakage flux into ETSP models. The first one assumes that since the leakage flux path is mostly air (discarding the effects of some magnetic materials besides the core, which

could be present inside the transformer), it can be assumed that the leakage inductances remain constant over time [7], [11]. The second approach incorporates the leakage flux paths in the magnetic lumped circuit as lumped reluctance elements (usually linear) that run parallel to the core leg reluctances [12], [13], [14].

Each of these two approaches has its advantages and disadvantages. Incorporating the leakage flux as constant inductances may only be feasible for two or three circuit transformers, and in addition, may lead to erroneous results when used to simulate events with heavy zero sequence components. This kind of lumped magnetic circuit does not take into account the air-tank wall space surrounding the windings, which constitutes the natural path for zero sequence fluxes in the case of three-phase three-limb transformers. The use of linear reluctances running parallel to the core leg reluctances requires detailed information about the arrangement and dimensions of the windings. This information is often considered proprietary by the manufacturer, and therefore is not readily available to the final user.

The approach used here was the first one since the information required to calculate the leakage inductances can usually be found in the transformer factory test reports. However, some information regarding the construction of the transformer core was still required. Additionally, in the case of five limb transformers the equivalent reluctance circuit still provides a path for zero sequence flux through the outer limbs (see Figure 5-2) as long as they do not reach saturation [15].

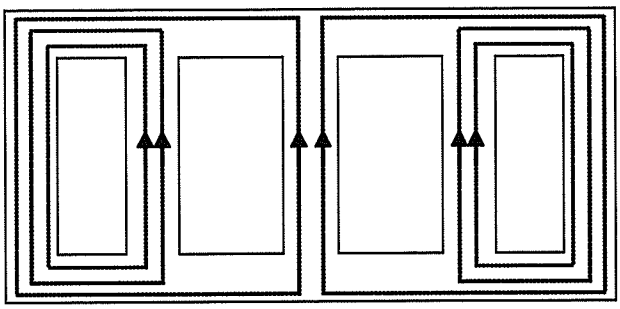

Figure 5-2 Zero sequence flux in a five-limb transformer (taken from [15])

Using this approach, the leakage flux linked by any of the primary windings can be written in terms of the leakage inductance $L_{H\sigma i}$ of the same winding, as follows

$$\phi_{H\sigma i} = \frac{L_{H\sigma i}}{n_H} i_{Hi} \qquad \text{Eq. 5.2}$$

Similar expressions can be derived for secondary and tertiary leakage fluxes.

By replacing systematically Eq. 5.2 into Eq. 5.1, the transformer voltage equations can be re-written as

$$\begin{aligned} v_{Hi} &= i_{Hi} r_{Hi} + L_{H\sigma i} \frac{di_{Hi}}{dt} + n_H \frac{d}{dt}[\Phi_i] \\ v_{Xi} &= i_{Xi} r_{Xi} + L_{X\sigma i} \frac{di_{Xi}}{dt} + n_X \frac{d}{dt}[\Phi_i] \\ v_{Yi} &= i_{Yi} r_{Yi} + L_{Y\sigma i} \frac{di_{Yi}}{dt} + n_Y \frac{d}{dt}[\Phi_i] \end{aligned} \qquad \text{Eq. 5.3}$$

This equation can in turn be written in matrix form as follows

$$\mathbf{V}(t)=\mathbf{r}\mathbf{i}(t)+\mathbf{L}_{\sigma}\frac{d}{dt}\left[\mathbf{i}(t)\right]+\mathbf{N}\frac{d}{dt}\left[\mathbf{\Phi}_{3\times1:3}(t)\right] \qquad \text{Eq. 5.4}$$

Where $\mathbf{r}$, $\mathbf{L}_{\sigma}$ and $\mathbf{N}$ are 9x9 diagonal matrices of the form

$$\mathbf{r}=\begin{bmatrix} r_{H1} & & & 0 \\ & r_{H2} & & \\ & & \cdots & \\ 0 & & & r_{Y3} \end{bmatrix},\quad \mathbf{L}_{\sigma}=\begin{bmatrix} L_{H\sigma1} & & & 0 \\ & L_{H\sigma2} & & \\ & & \cdots & \\ 0 & & & L_{Y\sigma3} \end{bmatrix},\quad \mathbf{N}=\begin{bmatrix} n_{H} & & & 0 \\ & n_{H} & & \\ & & \cdots & \\ 0 & & & n_{Y} \end{bmatrix} \qquad \text{Eq. 5.5}$$

$\mathbf{V}(t)$ and $\mathbf{i}(t)$ are vectors of the form

$$\mathbf{V}(t)^{T}=\begin{bmatrix} V_{H1} & V_{H2} & V_{H3} & V_{X1} & V_{X2} & V_{X3} & V_{Y1} & V_{Y2} & V_{Y3} \end{bmatrix} \qquad \text{Eq. 5.6}$$

$$\mathbf{i}(t)^{T}=\begin{bmatrix} i_{H1} & i_{H2} & i_{H3} & i_{X1} & i_{X2} & i_{X3} & i_{Y1} & i_{Y2} & i_{Y3} \end{bmatrix} \qquad \text{Eq. 5.7}$$

and where the $\mathbf{\Phi}_{3\times1:3}(t)$ vector is constructed by repeating three times the fluxes along the main limbs, as follows

$$\mathbf{\Phi}_{3\times1:3}(t)^{T}=\begin{bmatrix} \phi_1 & \phi_2 & \phi_3 & \phi_1 & \phi_2 & \phi_3 & \phi_1 & \phi_2 & \phi_3 \end{bmatrix} \qquad \text{Eq. 5.8}$$

which corresponds to the first three elements in the $\mathbf{\Phi}(t)$ vector, which is given by

$$\mathbf{\Phi}(t)^{T}=\begin{bmatrix} \phi_1 & \phi_2 & \phi_3 & \phi_4 \end{bmatrix}, \qquad \text{Eq. 5.9}$$

5.2 Equivalent lumped magnetic circuit

Due to magnetic non-linearity, the reluctance of the core material depends on the magnitude of the flux circulating through it. In modeling the equivalent lumped magnetic circuit the core was divided into sections, taking into consideration that the fluxes flowing through these sections should be approximately uniform. This was done in an effort to lump together portions of core with relatively homogeneous reluctances [8]. Figure 5-3 shows the arrangement chosen for the equivalent lumped magnetic circuit. Note that the leakage paths are not represented in this diagram since they were already considered as constant inductances in the voltage equations (see Eq. 5.3).

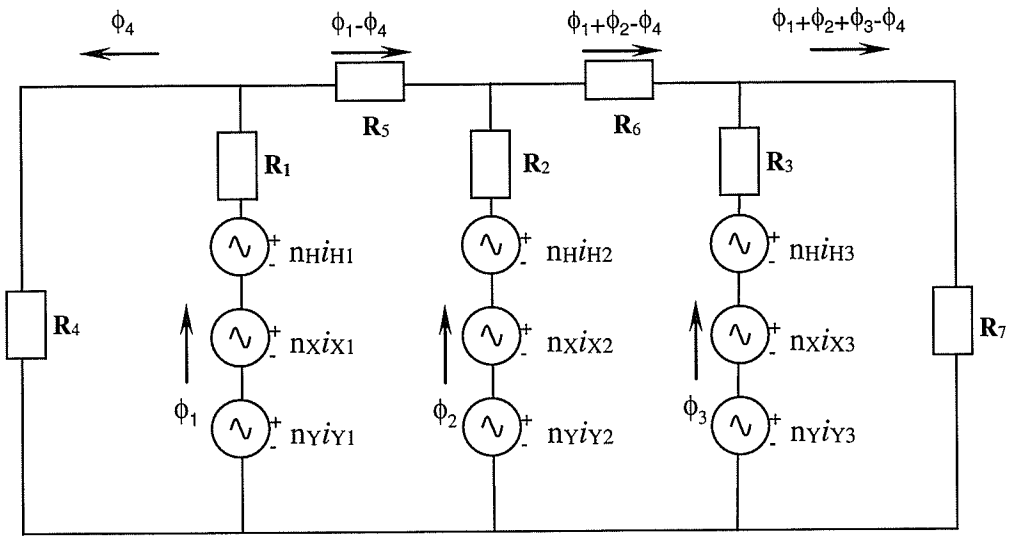

Figure 5-3 Five-limb transformer equivalent magnetic circuit

Loop equations can be written for the magnetic circuit on Figure 5-3 as follows

$$
\begin{aligned}
&n_H i_{H1} + n_X i_{X1} + n_Y i_{Y1} = \phi_1 R_1 + \phi_4 R_4 \\
&n_H i_{H1} + n_X i_{X1} + n_Y i_{Y1} - n_H i_{H2} - n_X i_{X2} - n_Y i_{Y2} = \phi_1 R_1 + (\phi_1 - \phi_4) R_5 - \phi_2 R_2 \\
&n_H i_{H2} + n_X i_{X2} + n_Y i_{Y2} - n_H i_{H3} - n_X i_{X3} - n_Y i_{Y3} = \phi_2 R_2 + (\phi_1 + \phi_2 - \phi_4) R_6 - \phi_3 R_3 \\
&n_H i_{H3} + n_X i_{X3} + n_Y i_{Y3} = \phi_3 R_3 + (\phi_1 + \phi_2 + \phi_3 - \phi_4) R_7
\end{aligned}
$$

Eq. 5.10

The magnetic circuit, as well as the loop equations above described is based on the assumption that the magnetomotive force across a given section of material equals the flux times the reluctance of the flux path (see equation bellow).

$$F = \phi R \qquad \text{Eq. 5.11}$$

where the reluctance is given by

$$R = \frac{l}{\mu A} \qquad \text{Eq. 5.12}$$

and where l and A are the length and area of the material under study.

This expressions (Eq. 5.11 and Eq. 5.12) are only valid for linear materials. However, they can be extended to non-linear materials if the reluctance is replaced with and equivalent instantaneous reluctance Req(t), as is shown in the next section.

5.2.1 Equivalent instantaneous reluctance

Ignoring hysteresis effects in the core material, an expression for the instantaneous reluctance can be found by approximating the B-H curve by means of linear splines (see

Figure 5-4). The mathematical formulation of the model is more straightforward when plotted as F-ϕ (Figure 5-5).

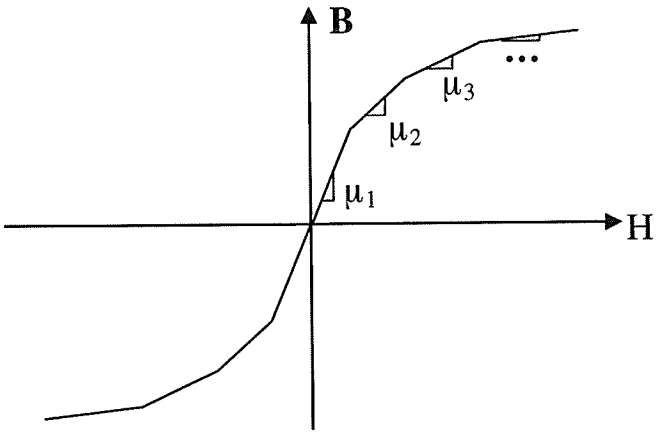

Figure 5-4 Linear splines B-H curve

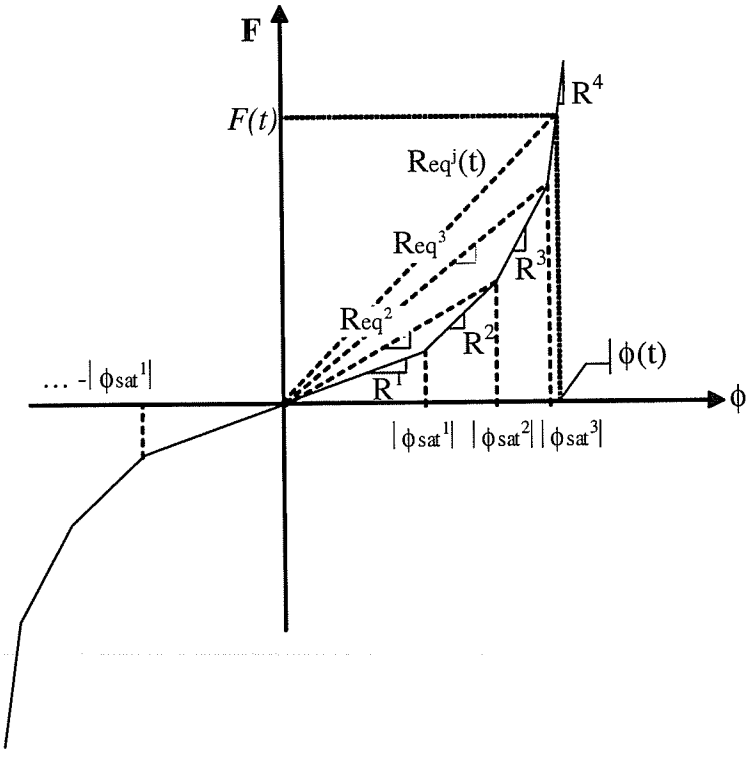

Figure 5-5 Linear splines F-ϕ curve

Based on Eq. 5.11 and Figure 5-5 an instantaneous equivalent reluctance Req(t) can be defined for non-linear magnetic materials as follows

$$Req^{j}(t)=\frac{R^{j}\phi(t)+\left[Req^{j-1}-R^{j}\right]\phi sat^{j-1}}{\phi(t)} \qquad \text{if } \left|\phi sat^{j-1}\right|\le\left|\phi(t)\right|<\left|\phi sat^{j}\right| \qquad \text{Eq. 5.13}$$

$$Req^{1}(t)=R^{1} \qquad \text{if } \left|\phi(t)\right|\le\left|\phi sat^{1}\right|$$

The final loop equations for the magnetic circuit can be obtained by replacing Eq. 5.13 into Eq. 5.10 and then writing in matrix form

$$\mathbf{n}\,\mathbf{i}(t)=\mathbf{R}^{j}(t)\boldsymbol{\Phi}(t)+\mathbf{F}^{\text{sat}}(t) \qquad \text{Eq. 5.14}$$

where

$$\mathbf{n}=\begin{bmatrix} n_H & 0 & 0 & n_X & 0 & 0 & n_Y & 0 & 0 \\ n_H & -n_H & 0 & n_X & -n_X & 0 & n_Y & -n_Y & 0 \\ 0 & n_H & -n_H & 0 & n_X & -n_X & 0 & n_Y & -n_Y \\ 0 & 0 & n_H & 0 & 0 & n_X & 0 & 0 & n_Y \end{bmatrix}, \qquad \text{Eq. 5.15}$$

$$\mathbf{R}^{j}(t)=\begin{bmatrix} R^{j}{}_{1} & 0 & 0 & R^{j}{}_{4} \\ R^{j}{}_{1}+R^{j}{}_{5} & -R^{j}{}_{2} & 0 & -R^{j}{}_{5} \\ R^{j}{}_{6} & R^{j}{}_{2}+R^{j}{}_{6} & -R^{j}{}_{3} & -R^{j}{}_{6} \\ R^{j}{}_{7} & R^{j}{}_{7} & R^{j}{}_{3}+R^{j}{}_{7} & -R^{j}{}_{7} \end{bmatrix}, \qquad \text{Eq. 5.16}$$

and

$$\mathbf{F}^{sat}(t)=\begin{bmatrix} \phi sat_1^{j-1}\left(Req_1^{j-1}-R_1^j\right)+\phi sat_4^{j-1}\left(Req_4^{j-1}-R_4^j\right) \\ \phi sat_1^{j-1}\left(Req_1^{j-1}-R_1^j\right)+\phi sat_5^{j-1}\left(Req_5^{j-1}-R_5^j\right)-\phi sat_2^{j-1}\left(Req_2^{j-1}-R_2^j\right) \\ \phi sat_2^{j-1}\left(Req_2^{j-1}-R_2^j\right)+\phi sat_6^{j-1}\left(Req_6^{j-1}-R_6^j\right)-\phi sat_3^{j-1}\left(Req_3^{j-1}-R_3^j\right) \\ \phi sat_3^{j-1}\left(Req_3^{j-1}-R_3^j\right)+\phi sat_7^{j-1}\left(Req_7^{j-1}-R_7^j\right) \end{bmatrix} \quad \text{Eq. 5.17}$$

With $j=1,2,\ldots,n$ splines, $\phi sat_k^0=0$ and $Req_k^0=0$

The flux vector can be found by solving Eq. 5.14, which gives

$$\mathbf{\Phi}(t)=\mathbf{R}^j(t)^{-1}\left[\mathbf{n}\,\mathbf{i}(t)-\mathbf{F}^{\mathbf{sat}}(t)\right] \quad \text{Eq. 5.18}$$

5.3 ETSP Implementation

As in the contactor case, in order to implement the transformer equations (Eq. 5.4) in the ETSP, a solution must be found in terms of time step increments. The trapezoidal approach is again chosen as the integration method.

Reorganizing Eq. 5.4 as follows

$$\left[\mathbf{V}(t)-\mathbf{r}\mathbf{i}(t)\right]dt=\mathbf{L}_\sigma d\mathbf{i}(t)+\mathbf{N}d\mathbf{\Phi}_{3\times1:3}(t) \quad \text{Eq. 5.19}$$

Eq. 5.19 can be integrated between t-Δt and t as per Eq. 1.3, which yields to

$$\frac{\Delta t}{2}\left[\mathbf{V}(t)+\mathbf{V}(t-\Delta t)\right]-\frac{\Delta t}{2}\mathbf{r}\left[\mathbf{i}(t)+\mathbf{i}(t-\Delta t)\right]=\mathbf{L}_\sigma\left[\mathbf{i}(t)-\mathbf{i}(t-\Delta t)\right]+\mathbf{N}\left[\mathbf{\Phi}_{3\times1:3}(t)-\mathbf{\Phi}_{3\times1:3}(t-\Delta t)\right] \quad \text{Eq. 5.20}$$

Where the main legs fluxes $\mathbf{\Phi}_{3\times1:3}(t)$ can be written in extended form by rewriting Eq. 5.18 three times for the three first fluxes as follows

$$\mathbf{\Phi}_{3\times1:3}(t)=\left[\mathbf{R}^{j}(t)^{-1}\,\mathbf{n}\right]_{3\times1:3}\mathbf{i}(t)-\left[\mathbf{R}^{j}(t)^{-1}\,\mathbf{F}^{\text{sat}}(t)\right]_{3\times1:3} \qquad \text{Eq. 5.21}$$

The currents are found by replacing Eq. 5.21 into Eq. 5.20 and solving for $\mathbf{i}(t)$. This gives

$$\mathbf{i}(t)=\mathbf{C}(t)^{-1}\left[\mathbf{Q}(t)+\mathbf{D}(t-\Delta t)+\mathbf{N}\mathbf{\Phi}_{3\times1:3}(t-\Delta t)\right] \qquad \text{Eq. 5.22}$$

where

$$\mathbf{D}(t-\Delta t)=\mathbf{V}(t-\Delta t)\frac{\Delta t}{2}+\left[\mathbf{L}_{\sigma}-\frac{\Delta t}{2}\mathbf{r}\right]\mathbf{i}(t-\Delta t)\,, \qquad \text{Eq. 5.23}$$

$$\mathbf{C}(t)=\frac{\Delta t}{2}\mathbf{r}+\mathbf{L}_{\sigma}+\mathbf{N}\left[\mathbf{R}^{j}(t)^{-1}\mathbf{n}\right]_{3\text{x}1:3} \qquad \text{Eq. 5.24}$$

and

$$\mathbf{Q}(t)=\mathbf{V}(t)\frac{\Delta t}{2}+\mathbf{N}\left[\mathbf{R}^{j}(t)^{-1}\,\mathbf{F}^{\text{sat}}(t)\right]_{3\times1:3} \qquad \text{Eq. 5.25}$$

In the implementation of the ETSP an initial state was assumed for the reluctances (usually the unsaturated state). Next the winding currents were calculated following Eq. 5.22. Knowing the current values was then possible to calculate the fluxes flowing through the reluctances. Depending on the magnitude of the fluxes, the program checked

at this point if any of the reluctances changed state (spline segment). If a change was found to happen, the currents were recalculated before proceeding to the next time step by repeating the whole cycle until the reluctances did not change spline segment. Figure 5-6 shows the flowchart implemented in the ETSP. In this case, no commercially available ETSP programs were used. Instead, an *Ad hoc* electromagnetic simulation program was written using Matlab code.

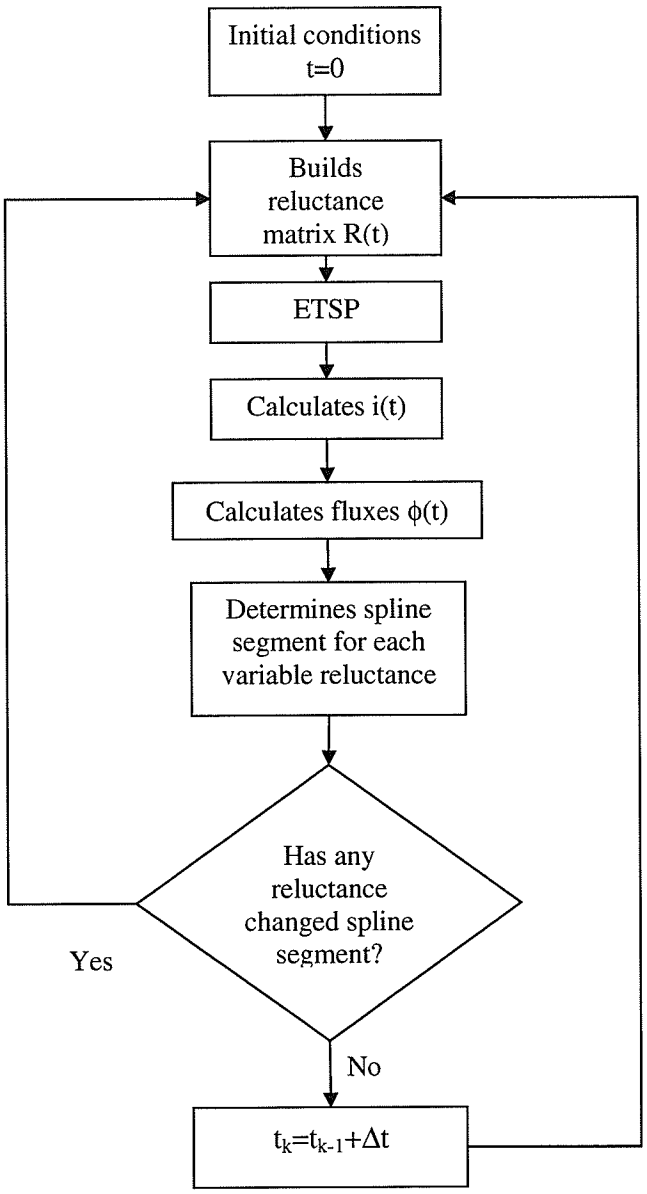

Figure 5-6 ETSP flowchart

5.4 Case study

Following the same technique used to analyze the performance of the PSCAD contactor model, some tests or scenarios were run for both transformer models, the finite element model and the coupled magnetic-electric lumped circuits model.

In the first instance, it was of interest to analyze the impact of the saturation level on the magnetizing current under steady state.

5.4.1 Physical description

As mentioned above, the transformer modeled has three circuits, a primary or high voltage circuit H and two low voltage circuits which are referred as secondary X and tertiary Y. All circuits H, X and Y are star connected.

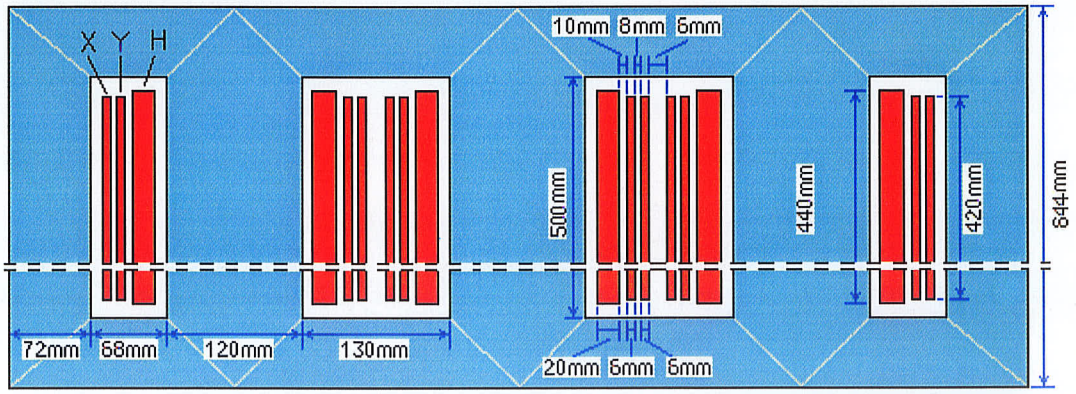

Figure 5-7 General layout of the three-phase five-limb transformer under study

The dimensions of the transformer studied are given in Figure 5-7. The values of some of the transformer's construction and electrical parameters were

$N_1 = 44$	number of turns in primary coil
$N_{2,3} = 4$	number of turns in secondary and tertiary windings, respectively
$r_1 = 5.6\ m\Omega$	primary windings resistance
$r_{2,3} = 157\ \mu\Omega$	Secondary and tertiary windings resistance
A_1, A_2, & $A_3 = 14011\ mm^2$	area of transformer main core legs
A_4, A_5, A_6 & $A_7 = 8407\ mm^2$	area of core yokes and outer legs
$Vn_H = 400$ V RMS	nominal line to line high voltage
Bn = 1.686 T	nominal main limbs flux density at 50 Hz

The core material was assumed to be magnetic steel with isotropic non-linear permeability. Its saturation curve was described using Eq. 3.1, with saturation flux density B_S=2.06T, initial relative permeability μ_r=2700 and bend adjustment coefficient a=0.05. For the purpose of the ETSP model, the B-H curve was approximated with a 10-segment linear spline curve. The segments within the spline curve were arbitrarily chosen to be grouped in the non-linear region and sparse in the quasi-linear regions. Figure 5-8 displays both, the original and the approximated curves.

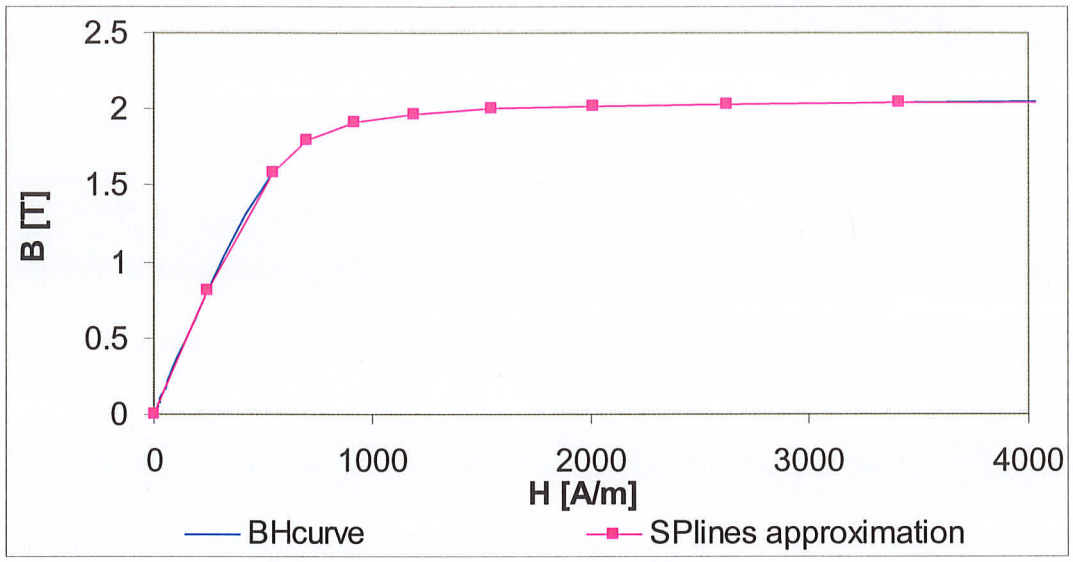

Figure 5-8 Core material B-H curve and its splines approximation

5.4.2 Quasi-steady state analysis

The quasi-steady state performance of the model was analyzed for low and high saturation levels. In this analysis, the transient simulations were run long enough until they converged to steady state.

The quantities measured were phase currents and ϕ_1, ϕ_2, ϕ_3 and ϕ_4 fluxes (ϕ_5, ϕ_6 and ϕ_7 can be found by combining the first four fluxes). In the case of the Finite Element model, the flux densities used in the comparison between both models were found by averaging the flux density along the paths shown in Figure 5-9.

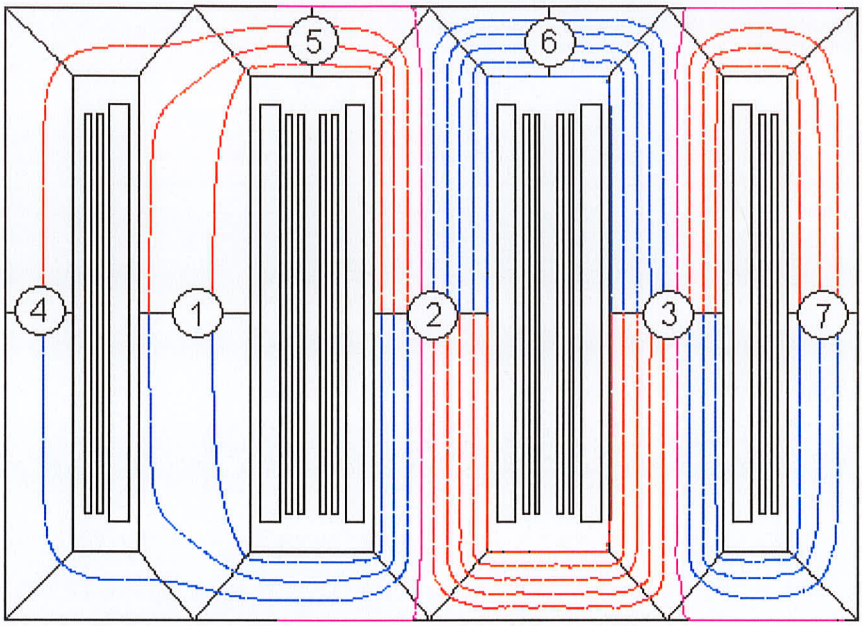

Figure 5-9 Flux density measurement locations

Figure 5-10 shows the results of such simulations. It can be observed that for the low saturation case (1.0 p.u. voltage), there is only a considerable difference (32.4%) in the current magnitude of the center limb (identified in Figure 5-9 as No. 2); even though both wave shapes display great similitude. The difference between core flux densities is barely appreciable.

Conversely, in the high saturation case (1.5 p.u. voltage), current magnitudes as well as wave shapes presented considerable discrepancies (see Table 5-1). Some difference in the flux density of the most left leg (identified in Figure 5-9 as No. 4) started to be appreciated.

Quantity	FEM	Lumped model	Difference
Ia	1239 A	718 A	72.4%

Quantity	FEM	Lumped model	Difference
Ib	1199 A	727 A	64.9 %
Ic	1167 A	628 A	85.8%

Table 5-1 Comparison between primary currents peak values: FEM vs. Lumped model

Richard *et al* [14] in a similar study found that currents calculated with two-dimensional transient FE differed up to 140% when compared against models based on coupled electric and magnetic lumped circuits. Their explanation for such differences was based on the fact that while 2D FE is a good method for analyzing core saturation, it gives a poor representation of the leakage flux, which follows a three-dimensional distribution.

This explanation could apply to the findings on the presented electromagnetic simulation. In the transient FE the leakage flux follows a two dimensional distribution, while the leakage inductances used in the lumped circuit were calculated by means of two-dimensional FE axi-symmetric analysis[4], which allows for an approximated 3D study of the flux distribution..

In order to really evaluate the impact of simplifying the geometry through the use of a lumped magnetic circuit linked to a lumped electric circuit it is necessary to make a comparison where both methods use the same basis. It would then be necessary to carry

---

[4] Axi-symmetric simulations have been widely used in the transformer industry. This method is regarded to yield quite accurate results when calculating leakage impedances, with typical errors smaller than 3%.

out transient 3D FEA of the five-limb transformer. However, due to the fact that the available FEA program was only 2D, this was not possible. In the special case of a two-winding transformer with a central limb, an axi-symmetric formulation is possible which gives 3D results with a 2D program. This is the subject of the next chapter.

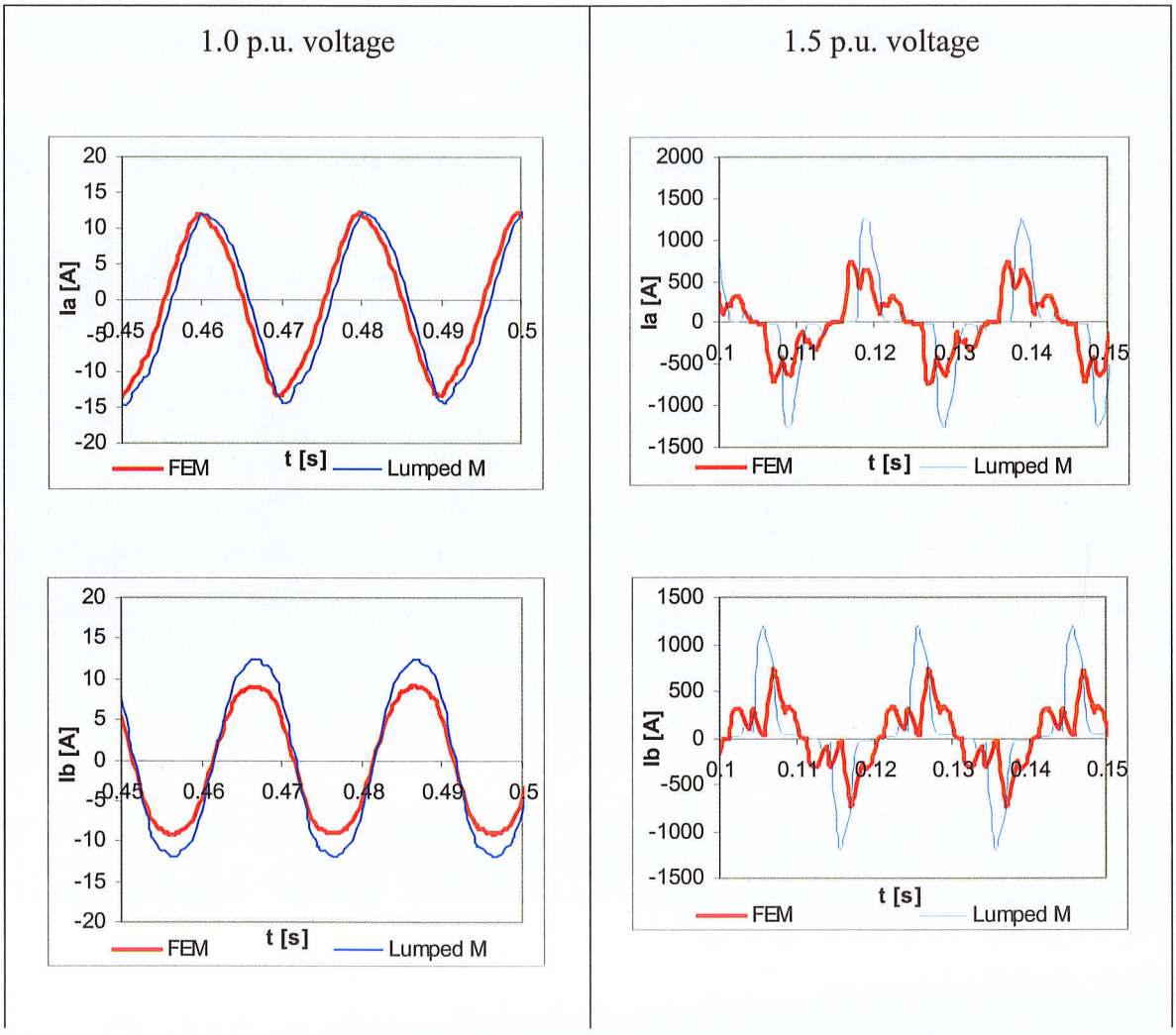

1.0 p.u. voltage	1.5 p.u. voltage
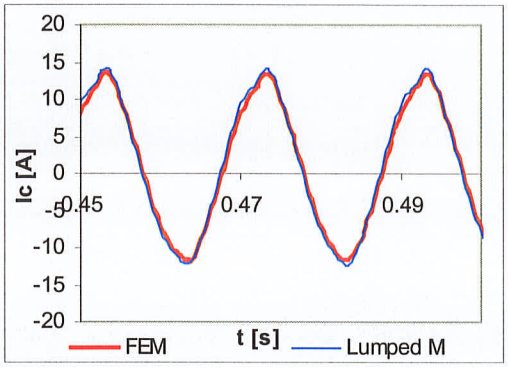	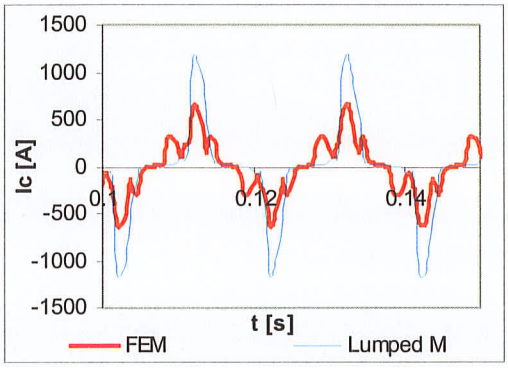
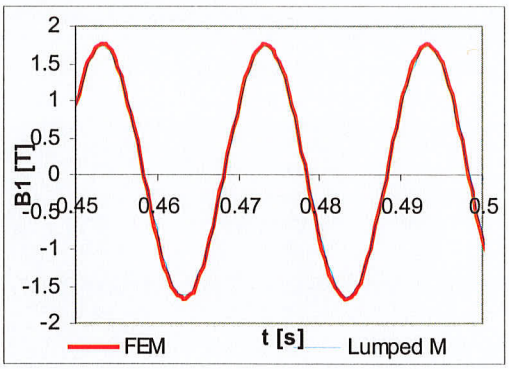	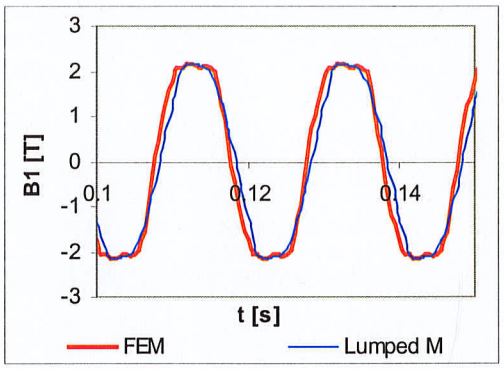
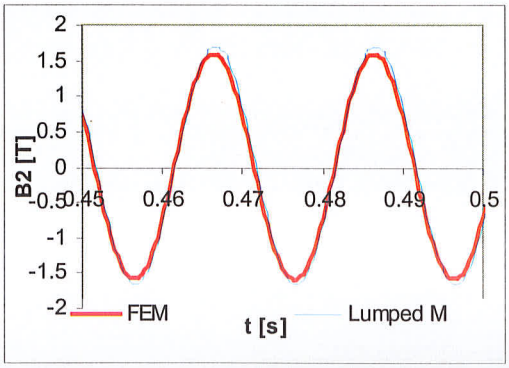	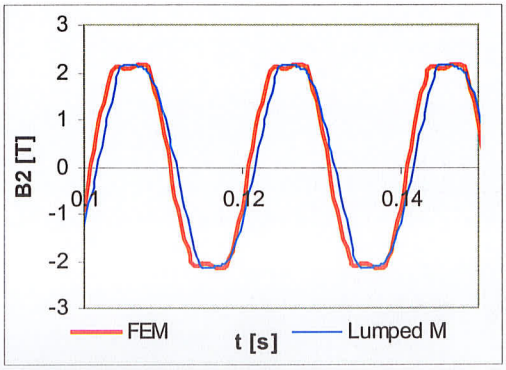

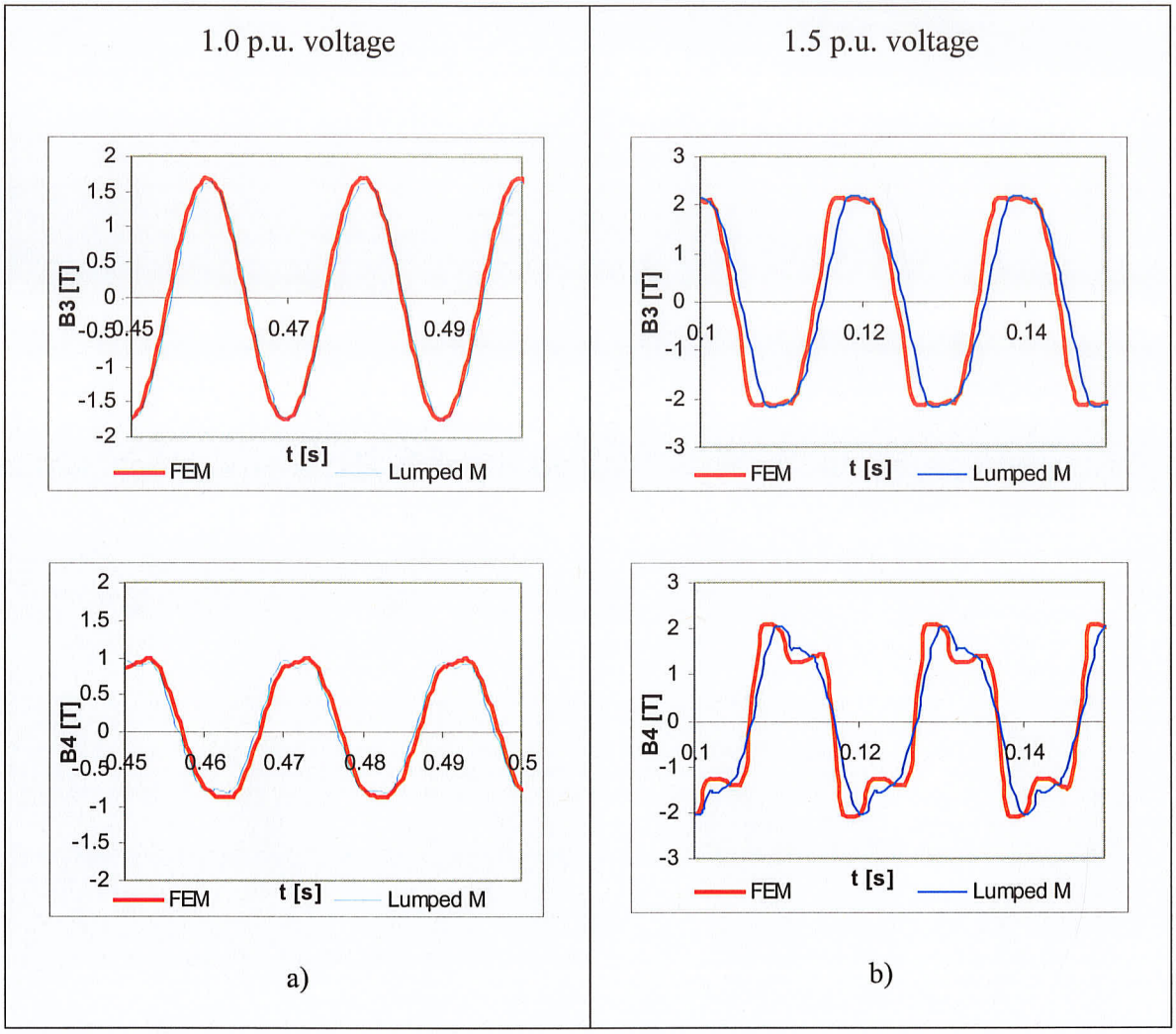

Figure 5-10 Quasi-steady state response of The 5-limb transformer when excited with a) 1.0 p.u. voltage b) 1.5 p.u. voltage

6 TRANSIENT ANALYSIS: THE SINGLE-PHASE TWO-CIRCUIT TRANSFORMER

The findings of the previous chapter pointed out the need for carrying out a comparison where both, the ETSP and the transient FE simulation are based on three-dimensional modeling techniques. For this purpose a simpler case was selected: a two-circuit single-phase transformer. Again, no commercially available ETSP were used. The magneto-electric equations are solved using *Ad hoc* electromagnetic programs written using Matlab code.

The lumped magnetic and electric circuit model was built utilizing two different approaches. In the first one, the leakage flux was represented as constant inductances in the electric circuit (as is often the practice [7], [11]). In the second one, the leakage flux was modeled as part of the magnetic circuit by providing a series of leakage reluctances [12], [13], [14].

The transient FE program used to validate the results, as it was mentioned in Chapter 5, was a 2D FE engine in axi-symmetric mode. In this mode, a 3D distribution of the flux can be approximated following the symmetry and simplicity of the two-winding transformer under study.

The performance of both lumped models was evaluated by comparing their results against the transient FE simulation for an inrush case. It will be seen later that only the second approach, the one that models the leakage flux as part of the magnetic circuit, yields acceptable results.

6.1 Lumped model with constant leakage inductances

The transformer voltage equations using constant inductances for the leakage flux are given by

$$v_1 = i_1 r_1 + L_{\sigma 1}\frac{di_1}{dt} + n_1\frac{d}{dt}[\Phi_1] \qquad \text{Eq. 6.1}$$

$$v_2 = i_2 r_2 + L_{\sigma 2}\frac{di_2}{dt} + n_2\frac{d}{dt}[\Phi_1]$$

and the magnetic circuit equation is given by

$$n_1 i_1 + n_2 i_2 = \phi_1 R_1 \qquad \text{Eq. 6.2}$$

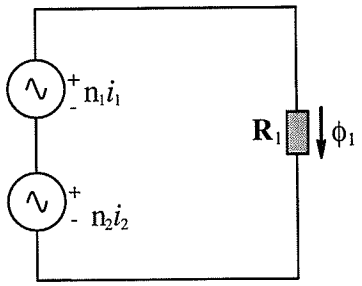

Figure 6-1 Single-phase transformer equivalent magnetic lumped circuit (first approach)

The solution for the currents and flux is found using the same procedure as in the previous chapter. This gives

$$\mathbf{i}(t) = \mathbf{C}(t)^{-1}\left[\mathbf{Q}(t) + \mathbf{D}(t-\Delta t) + \mathbf{N}\boldsymbol{\Phi}_{x2}(t-\Delta t)\right] \qquad \text{Eq. 6.3}$$

$$\phi_1(t) = \frac{n_1 i_1 + n_2 i_2}{R_1^{\,j}(t)} - \frac{1}{R_1^{\,j}(t)}\left[Req_1^{\,j-1} - R_1^{\,j}\right]\phi sat_1^{\,j-1} \qquad \text{Eq. 6.4}$$

where

$$\mathbf{C}(t) = \mathbf{L}_\sigma + \frac{\Delta t}{2}\mathbf{r} + \frac{1}{R_1^{\,j}}\mathbf{N}\,\mathbf{n}, \qquad \text{Eq. 6.5}$$

$$\mathbf{D}(t-\Delta t) = \frac{\Delta t}{2}\mathbf{V}(t-\Delta t) + \left[\mathbf{L}_\sigma - \frac{\Delta t}{2}\mathbf{r}\right]\mathbf{i}(t-\Delta t)$$

and

$$\mathbf{Q}(t) = \frac{\Delta t}{2}\mathbf{V}(t) + \frac{1}{R_1^{\,j}}\mathbf{N}\,F^{sat}$$

with

$$\boldsymbol{\Phi}_{x2}(t) = \begin{bmatrix}\phi_1(t)\\ \phi_1(t)\end{bmatrix},$$

$$\mathbf{r} = \begin{bmatrix} r_1 & 0 \\ 0 & r_2 \end{bmatrix}, \quad \mathbf{L}_\sigma = \begin{bmatrix} L_{\sigma 1} & 0 \\ 0 & L_{\sigma 2} \end{bmatrix}, \quad \mathbf{N} = \begin{bmatrix} n_1 & 0 \\ 0 & n_2 \end{bmatrix}, \quad \mathbf{n} = \begin{bmatrix} n_1 & n_2 \\ n_1 & n_2 \end{bmatrix}$$

and

$$F^{sat}(t) = \phi sat_1^{j-1}\left(Req_1^{j-1} - R_1^j\right)$$

6.2 Lumped model using reluctances for the leakage paths

In this model the paths for the leakage flux are provided as leakage reluctances. Figure 6-2 shows the reluctances as well as the fluxes taken into account during the modeling stage. Here the direction of the fluxes have been drawn as if the outer winding was the primary winding with a magnetomotive force (mmf) slightly higher than the inner winding's mmf.

Figure 6-3 shows the equivalent magnetic circuit. The darkened boxes are representation of flux paths that flow trough non-linear reluctances. Note that the tank flux ϕ_3 has been assigned to a non-linear reluctance R_3, as in most cases the tank is built with magnetic steel material.

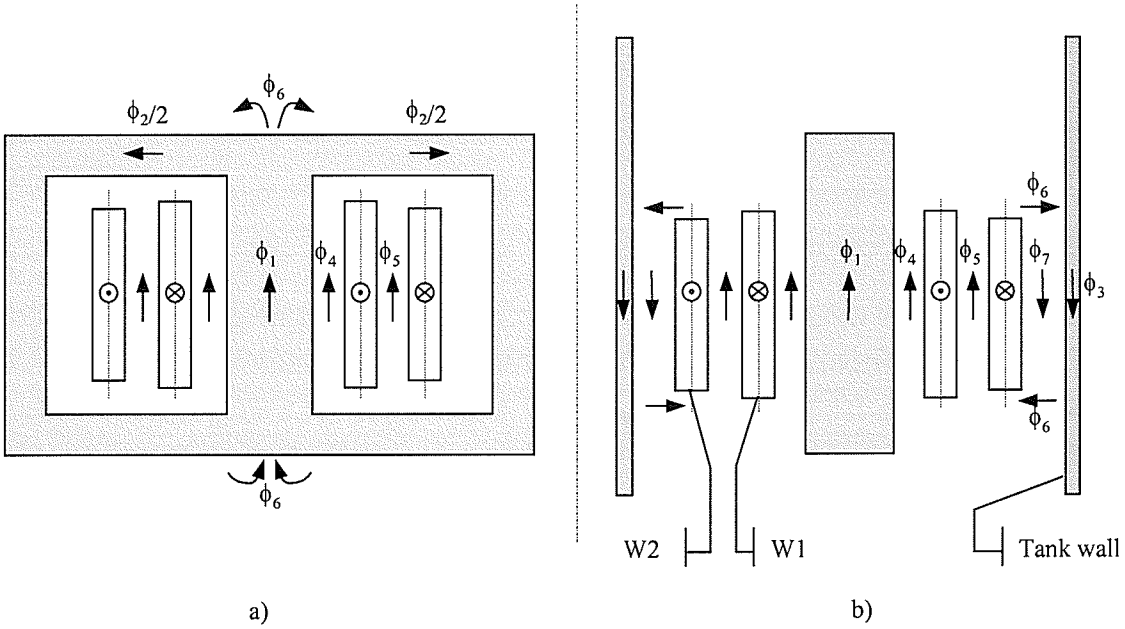

Figure 6-2 Flux distribution on a single-phase two winding core-type transformer with outer winding mmf slightly higher than inner winding mmf. a) Front view. b) Side view

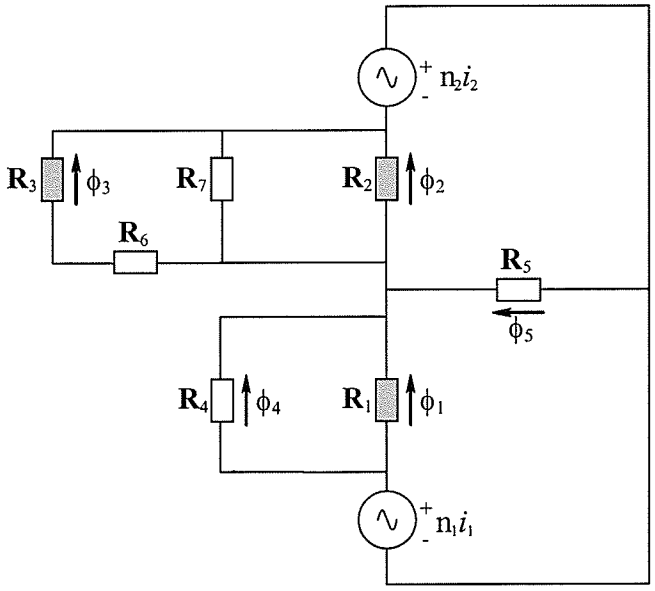

Figure 6-3 Single-phase transformer equivalent magnetic lumped circuit (second approach)

The transformer voltage equations are written as

$$v_1 = i_1 r_1 + n_1 \frac{d}{dt}\left[\Phi_1 + \Phi_{\sigma 1}\right] \qquad \text{Eq. 6.6}$$
$$v_2 = i_2 r_2 + n_2 \frac{d}{dt}\left[\Phi_1 + \Phi_{\sigma 2}\right]$$

Where the leakage fluxes are given by

$$\Phi_{\sigma 1} = \Phi_4 \qquad \text{Eq. 6.7}$$
$$\Phi_{\sigma 2} = \Phi_4 + \Phi_5$$

The loop equations for the magnetic circuit on Figure 6-3 are given by

$$-n_1 i_1 = \phi_1 R_1 - \phi_5 R_5 \qquad \text{Eq. 6.8}$$
$$n_2 i_2 = \phi_2 R_2 + \phi_5 R_5$$
$$0 = \phi_1 R_1 - \phi_4 R_4$$
$$0 = \phi_2 R_2 + \left(-\phi_1 + \phi_2 + \phi_3 - \phi_4 - \phi_5\right) R_7$$
$$0 = \phi_2 R_2 - \left(R_3 + R_6\right)\phi_3$$

Expressions for currents and fluxes can be found by solving Eq. 6.6 and Eq. 6.8 by applying the trapezoidal approach, as follows

$$\mathbf{i}(t) = \mathbf{C}(t)^{-1}\left[\mathbf{Q}(t) + \mathbf{D}(t-\Delta t) + \mathbf{N}\boldsymbol{\Phi}_{\mathrm{W}}(t-\Delta t)\right] \qquad \text{Eq. 6.9}$$

$$\boldsymbol{\Phi}(t) = \mathbf{R}^{j}(t)^{-1}\left[\mathbf{n}\begin{bmatrix} i_1(t) \\ i_2(t) \\ 0 \\ 0 \\ 0 \end{bmatrix} + \mathbf{F}^{sat}(t)\right] \qquad \text{Eq. 6.10}$$

where

$$\mathbf{C}(t)=\frac{\Delta t}{2}\mathbf{r}+\mathbf{N}\,\mathbf{K}\,, \qquad \text{Eq. 6.11}$$

$$\mathbf{D}(t-\Delta t)=\frac{\Delta t}{2}\mathbf{V}(t-\Delta t)-\frac{\Delta t}{2}\mathbf{r}\,\mathbf{i}(t-\Delta t)\,,$$

$$\mathbf{Q}(t)=\frac{\Delta t}{2}\mathbf{V}(t)+\mathbf{N}\mathbf{P}^{\mathbf{sat}}$$

and

$$\mathbf{\Phi}_{\mathrm{W}}(t)=\begin{bmatrix}\phi_1(t)+\phi_4(t)\\ \phi_1(t)+\phi_4(t)+\phi_5(t)\end{bmatrix}$$

with

$$\mathbf{P}^{sat}=\begin{bmatrix}\left[\mathbf{R}^j(t)^{-1}\mathbf{F}^{sat}\right]_1+\left[\mathbf{R}^j(t)^{-1}\mathbf{F}^{sat}\right]_4\\ \left[\mathbf{R}^j(t)^{-1}\mathbf{F}^{sat}\right]_1+\left[\mathbf{R}^j(t)^{-1}\mathbf{F}^{sat}\right]_4+\left[\mathbf{R}^j(t)^{-1}\mathbf{F}^{sat}\right]_5\end{bmatrix},$$

$$\mathbf{K}=\begin{bmatrix}\left[\mathbf{R}^j(t)^{-1}\mathbf{n}\right]_{1,1}+\left[\mathbf{R}^j(t)^{-1}\mathbf{n}\right]_{4,1} & \left[\mathbf{R}^j(t)^{-1}\mathbf{n}\right]_{1,2}+\left[\mathbf{R}^j(t)^{-1}\mathbf{n}\right]_{4,2}\\ \left[\mathbf{R}^j(t)^{-1}\mathbf{n}\right]_{1,1}+\left[\mathbf{R}^j(t)^{-1}\mathbf{n}\right]_{4,1}+\left[\mathbf{R}^j(t)^{-1}\mathbf{n}\right]_{5,1} & \left[\mathbf{R}^j(t)^{-1}\mathbf{n}\right]_{1,2}+\left[\mathbf{R}^j(t)^{-1}\mathbf{n}\right]_{4,2}+\left[\mathbf{R}^j(t)^{-1}\mathbf{n}\right]_{5,2}\end{bmatrix},$$

$$\mathbf{F}^{sat}(t)=\begin{bmatrix} \phi sat_1^{j-1}\left(Req_1^{j-1}-R_1^j\right) \\ \phi sat_2^{j-1}\left(Req_2^{j-1}-R_2^j\right) \\ \phi sat_1^{j-1}\left(Req_1^{j-1}-R_1^j\right) \\ \phi sat_2^{j-1}\left(Req_2^{j-1}-R_2^j\right) \\ -\phi sat_2^{j-1}\left(Req_2^{j-1}-R_2^j\right)+\phi sat_3^{j-1}\left(Req_3^{j-1}-R_3^j\right) \end{bmatrix},$$

$$\mathbf{R}^j(t)=\begin{bmatrix} R^j{}_1 & 0 & 0 & 0 & -R_5 \\ 0 & R^j{}_2 & 0 & 0 & R_5 \\ R^j{}_1 & 0 & 0 & -R_4 & 0 \\ -R_7 & R^j{}_2+R_7 & R_7 & -R_7 & -R_7 \\ 0 & -R^j{}_2 & R^j{}_3+R_6 & 0 & 0 \end{bmatrix},$$

and

$$\mathbf{n}=\begin{bmatrix} n_1 & 0 & 0 & 0 & 0 \\ 0 & n_2 & 0 & 0 & 0 \\ 0 & 0 & 0 & 0 & 0 \\ 0 & 0 & 0 & 0 & 0 \\ 0 & 0 & 0 & 0 & 0 \end{bmatrix},\ \mathbf{N}=\begin{bmatrix} n_1 & 0 \\ 0 & n_2 \end{bmatrix} \text{ and } \mathbf{r}=\begin{bmatrix} r_1 & 0 \\ 0 & r_2 \end{bmatrix}$$

The leakage reluctances were calculated according to the physical geometry of the flux paths by using

$$R=\frac{l}{\mu A}K \qquad \text{Eq. 6.12}$$

where K is the winding Rogowky's factor given by

$$K = 1 - \frac{2RB + ID}{\pi\, h} \qquad \text{Eq. 6.13}$$

with RB as the radial build, ID the inner diameter and h the height of the winding.

For the purpose of comparing similar arrangements against the FE simulation, the reluctances in the lumped model were calculated using a perfectly cylindrical configuration, like the one depicted in Figure 4-4 for the FE geometrical setup.

6.3 Simulation results

In order to test both models, a transient scenario known as the inrush phenomena was chosen. Appendix B provides a brief introduction on this type of events. In the simulated case the transformer was energized at the beginning of the voltage cycle $V = V_{MAX}\sin(\omega t)$, with the core holding a remanent flux of 1 Tesla.

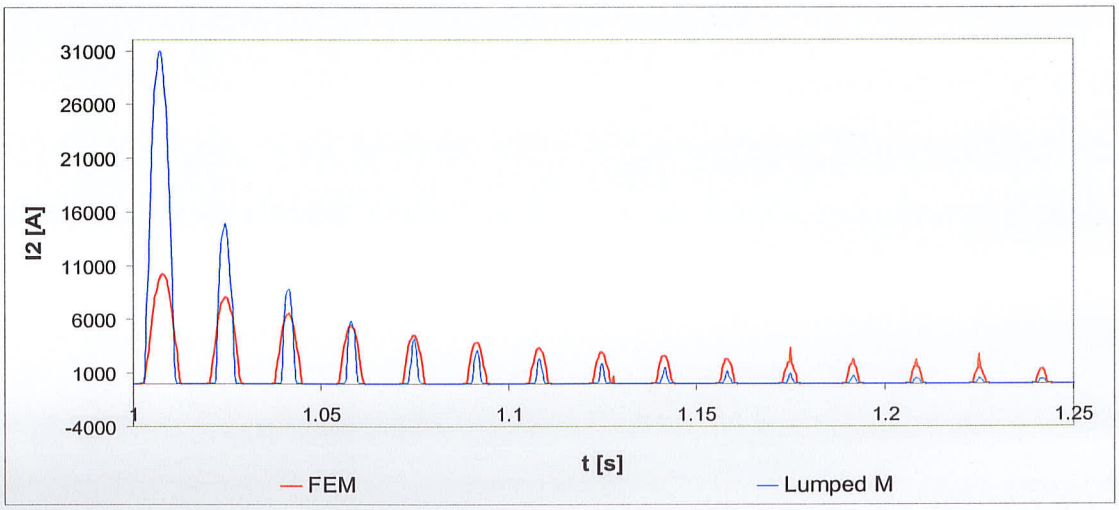

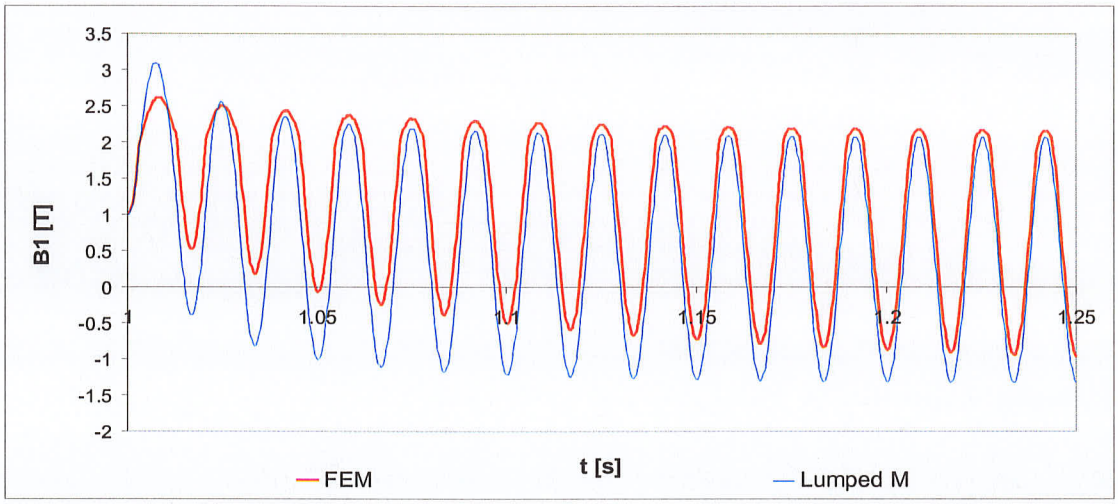

Figure 6-4 FEM vs. Lumped circuit model using constant leakage inductances: Current of primary coil I_2 and flux density along main core leg ϕ_1

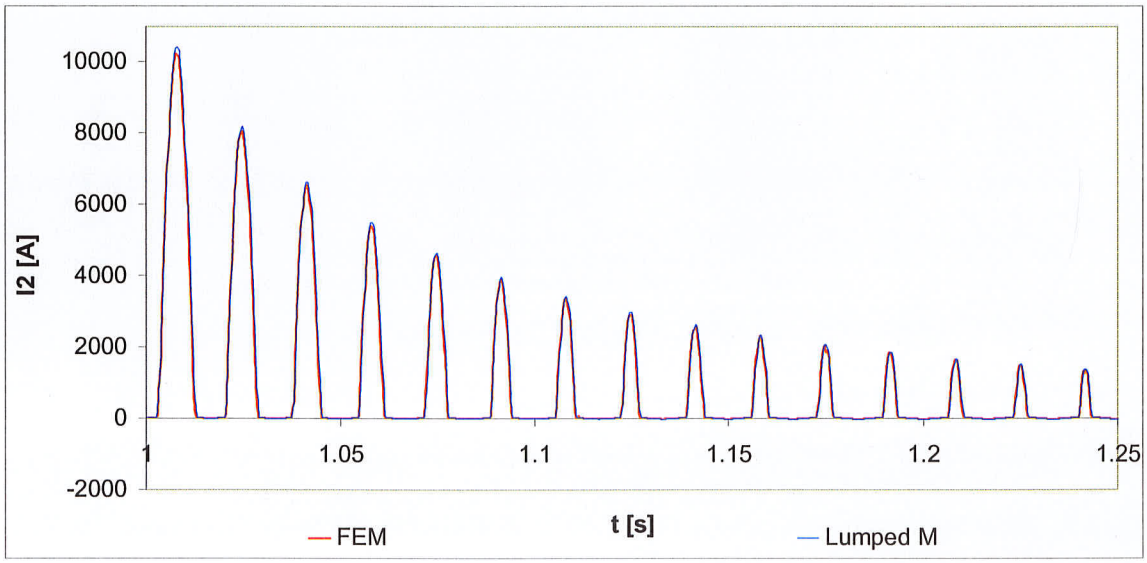

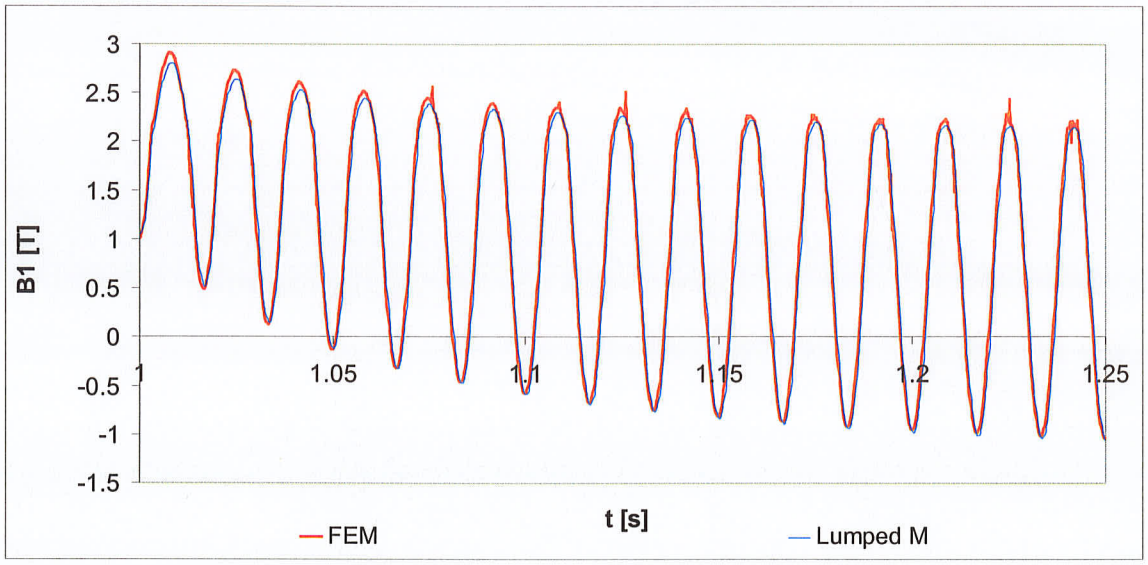

Figure 6-5 FEM vs. Lumped circuit model using reluctances for leakage fluxes paths: Current of primary coil I_2 and flux density along main core leg ϕ_1

The comparison between the transient FE and the lumped circuit with constant leakage inductances is given in Figure 6-4. Here it can be observed that there is a very high difference between the two methods, especially for the currents, where the magnitude of the first peak in the lumped model is approximately three times higher than the FE one.

On the other hand, Figure 6-5 shows a very different outcome when the leakage reluctances are incorporated in the magnetic circuit. In this case the differences between calculated values are of only 2.1% and 3.4% for the first peak of the current and the main flux, respectively. This result suggests that the modeling method to use when simulating inrush events in transformers is to incorporate the leakage fluxes as part of the lumped magnetic circuit.

In order to check the repeatability of these results, a second simulation was performed for another two-winding single-phase transformer (see Appendix 3). The model was tested as well using the inner winding as primary winding. Table 6-1 summarizes the results for these simulations. No difference was found to surpass 10%.

Transformer	Primary winding	Remanant flux density	Primary winding current first peak difference	Flux first peak difference
1	Inner winding	1.0 T	8.5 %	4.9%
	Outer winding	1.0 T	2.1 %	3.4 %
2	Inner winding	1.68 T	1.6 %	5.6 %
	Outer winding	1.59 T	5.7 %	9.3%

Table 6-1 Single-phase transformer inrush simulation. FEM vs. Lumped model with reluctances for leakage fluxes

7 CONCLUSIONS

- This thesis introduced a new approach for simulating transient events in non-linear electromagnetic systems by using FEA and ETSP in a decoupled manner. In the simulated systems, the introduced approach was found to drastically reduce simulation times as it was shown in Chapter 3. This approach can be incorporated into large ESTP solver, hence, allowing the study of complicated electromagnetic networks.

- Very accurate results were obtained with the FEA-ETSP decoupled method in simulating transient events where the role of eddy currents did not significantly affect the performance of the electromagnetic system.

  It was also found that the method's accuracy is directly linked to the quality or sampling level of the non-linear inductance mapped model. The better the quality of the mapped model, the higher the accuracy of the transient simulation.

- A drawback found on the FEA-ETSP decoupled method was the amount of resources needed for the construction of the mapped non-linear model, particularly when the number of windings is large. This constraint limits the feasibility of this method to simulating relatively simple non-linear electromagnetic systems.

- In order to address the above drawback, and alternate approach for simulating more complex electromagnetic systems was studied. This approach used lumped magnetic circuits coupled to lumped electric circuits incorporating all the windings' leakage fluxes into the electric circuit as constant inductances. This method was used to model a three-phase three-circuit five-limb transformer. The performance of this model was compared against a 2D transient FEA model for different levels of core magnetization in the steady state. In this case, the non-linear lumped magnetic circuit produced similar results to the 2D FE simulation for low levels of core saturation. However, it was impossible to determine if the method is good for studying configurations with high saturation levels.

  It was found that 2D FE can not be used as a reliable reference when the core is saturated because the flux follows a 3D distribution under this state.

- Due to the simplicity of the electromagnetic system chosen in chapter 6, the two-circuit single-phase transformer allowed for a simplified 3D analysis with the available transient 2D FE engine. With this case it was possible to show that using lumped magnetic circuits coupled to electric circuits while using constant inductances[5] to represent leakage fluxes introduces considerable errors if used to simulate cases where the core is driven into high saturation. It was found that these

---

[5] The values of inductance used were found using the impedance voltage IeX%, which is generally provided by transformer manufacturers.

kind of electromagnetic systems are better modeled when the leakage flux paths are incorporated into the magnetic circuit.

7.1 Future work

- The possibility of introducing the handling of a non-linear element whose reluctance depends on the magnitude of the flux circulating through it would eliminate the necessity for writing the magnetic circuit equations in advance. Instead, it would be as simple as choosing a configuration that represents the magnetic circuit of the transformer under study and then drawing it in PSCAD. For this to be achievable a non-linear solving algorithm would have to be introduced. This would allow the possibility of simulating magnetic configurations of much higher complexity. The drawback would be a considerable reduction in computation speed since several iterations would be required for every time step.

- The transformer decoupled FEA-ETSP model and the transformer coupled lumped magnetic – electric circuits model need to be tested on a wider set of scenarios in order to identify their limitations as well as the types of applications where they perform the best.

- The inaccuracy of the model in Chapter 6 that used lumped magnetic circuits coupled to lumped magnetic circuits while using constant leakage inductances to represent leakage inductances at simulating high saturation cases suggests that the leakage inductances are also non-linear. The method introduced in Chapter 4 could be used to

indirectly measure leakage inductances under different core saturation levels, and therefore used to prove the non-linearity of the leakage inductances.

- Real laboratory experiments need to be performed in order to validate the findings in this thesis. This in regard to the accuracy of the decoupled FEA-ETSP method, as well as the coupled lumped magnetic and electric circuits method.

REFERENCES

[1] Reece, A. B. J., Preston, T.W. "Finite Element Methods in Electrical Power Engineering" Oxford University Press Inc., New York, 2000. IBSBN 0-19-856504-6

[2] Wang, H., Butler, K. L. "Finite Element Analysis of Internal Winding Faults in Distribution Transformers" IEEE Transaction on Power Delivery, Vol. 16, No. 3, July 2001.

[3] "Flux 2D 7.60/Flux 3D 3.3, User's Guide Volume 2: General Working of Flux 3D/Preflu_2D, Geometry and Mesh, Managing Circuits and Materials" Cedrat, France, December 2001.

[4] "Flux 2D Version 7.60, User's Guide Volume 3: Physical Properties, Parameterization, Solving and Results" Cedrat, France, November 2001.

[5] Hayt, William Hart "Engineering Electromagnetics" McGraw-Hill, 5th international edition, New York 1989, ISBN 0-07-027406-1

[6] Gole, Ani, "Course Notes: 24.731 Power Systems Transients Simulation" University of Manitoba, Spring 2003, http://www.ee.umanitoba.ca/~gole/24.731/

[7] Dolinar, D., Pihler, J., Grcar, B. "Dynamic Model of a Three-phase Power Transformer" IEEE Transactions on Power Delivery, Vol. 8, No. 4, October 1993.

[8] Yacamini, R., Bronzeado, H. "Transformer Inrush Calculations using a Coupled Electromagnetic Model" IEE Proceedings-Science, Measurements and Technology, Vol. 141, No. 6, November 1994.

[9] Jagdish Rao, Dattaraj. "The Finite Element Method Site", http://dattaraj_rao.tripod.com/FEM/tutorial.html

[10] Sadiku, Matthew N. O. "A Simple Introduction to Finite Element Analysis of Electromagnetic Problems" IEEE Transactions on Education. Vol. 32 No. 2, May 1989.

[11] Elrefaie, Hesham B., Megahed, Ashraf I. "Modeling Transformer Internal Faults Using Matlab" IEEE MELECON 2002, May 7-9, 2002, Cairo, Egypt.

[12] Dallago, E., Sassone, G., Venchi, G. "High-Frequency Power Transformer Model for Circuit Simulation" IEEE Transactions on Power Electronics, Vol. 12, No. 4, July 1997.

[13] Mohseni, H. "Multi-Winding Multi-Phase Transformer Model with Saturable Core" IEEE Transactions on Power Delivery, Vol. 6, No. 6, No. 1, January 1991.

[14] Richard, N., Szylowicz, N. "Comparison Between a Permeance Network Model and a 2D Finite Element Model for the Inrush Current Computation in a Three-

Phase Transformer" IEEE Transactions on Magnetics, Vol. 30, No. 5, September 1994.

[15] Ngneguey, T., Mailhot, M., Munar, A. "Zero Phase Sequence Impedance and Tank Heating Model for Three Phase Three Leg Core Type Power Transformers Coupling Magnetic Field and Electric Circuit Equations in a Finite Element Software" IEEE Transactions on Magnetics, Vol. 31, No. 3, May 1995.

[16] Dommel, H. W. "Digital Computer Solution of Electromagnetic Transients in Single and Multiphase Networks" IEEE Transactions PAS, Vol. PAS-88, No. 4, pp. 388-399, April 1969.

[17] Nordstrom, John Eric "Precise Modeling of Power Electronic Control Signals in Discrete Time Step Electromagnetic Transients Programs" Master's thesis, University of Manitoba, March 2004

Appendix 1 MAXWELL'S EQUATIONS

Maxwell's equations are a set of partial differential equations that relate electric and magnetic fields with their sources (electric charges or current densities). These describe the principles of guiding and propagation of electromagnetic energy and provide the fundamentals of the electromagnetic phenomena and its applications.

$$\vec{\nabla} \times \vec{E} = -\frac{\partial \vec{B}}{\partial t}$$ Eq. A 1

Faraday's Law

$$\vec{\nabla} \cdot \vec{H} = \rho_v$$ Eq. A 2

Gauss' Law

$$\vec{\nabla} \times \vec{H} = \vec{J} + \frac{\partial \vec{D}}{\partial t}$$ Eq. A 3

Ampere's Law

$$\vec{\nabla} \cdot \vec{B} = 0$$ Eq. A 4

where

$\vec{E}$ Electric field intensity [V/m]

$\vec{B}$	Magnetic field [T]
$\vec{D}$	Electric flux density [C/m^2]
ρ_V	Volumetric charge density [C/m^3]
$\vec{H}$	Magnetic field intensity [A/m]
$\vec{J}$	Current density [A/m^2]

In the Ampere's law $\vec{J}$ (Eq. A 4) is given by the summation of the source current density $\vec{J}_s$ and the induced current density $\vec{J}_e$. In the case of two-dimensional problems, the induced current density can be expressed as

$$J_e = -\sigma \frac{\partial A}{dt} \qquad \text{Eq. A 5}$$

where

$\vec{A}$	Vector magnetic potential [Wb/m]
σ	Conductivity [$\mho / m$]

The auxiliary equation that relates $\vec{D}$ with $\vec{E}$ is

$$\vec{D} = \varepsilon \vec{E} \qquad \text{Eq. A 6}$$

$\vec{B}$ with $\vec{H}$

$$\vec{B} = \mu \vec{H} \qquad \text{Eq. A 7}$$

and the conduction current density with the electric field

$$\vec{J_C} = \sigma \vec{E} \qquad \text{Eq. A 8}$$

where

ε	Electric permitivity [F/m]
μ	Magnetic permeability [H/m]

Appendix 2 THE INRUSH PHENOMENA

The voltage v across a winding in a transformer is given by the derivative of the flux linked ϕ by such winding, as per Eq. B 1.

$$v = \frac{d\phi}{dt} \qquad \text{Eq. B 1}$$

Under steady-state, voltage and linked flux have wave shapes as the ones represented on Figure B 1a

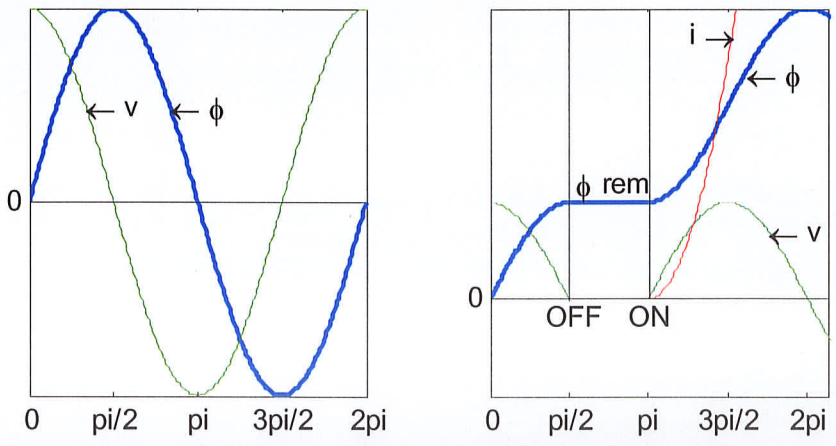

Figure B 1 Flux and voltage wave shape under: a) steady-state with non-saturated core. b) worst inrush scenario

When a transformer is switched off, depending on the point of the magnetizing curve at which it is de-energized, there could be some remnant flux on the core. For example, in Figure B 2, if the switch off takes place at point A, the current, and consequently the magnetic field intensity H will go to zero. The flux density will follow the core material hysteresis curve and will sit at the H zero crossing of the curve at the remnant flux density B_{rem}.

The worst inrush current scenario takes place when the switch *off* and *on* of the transformer is carried out at the zero voltage crossing, having these two instants opposite signs of the voltage tangent, as depicted on Figure B 1b.

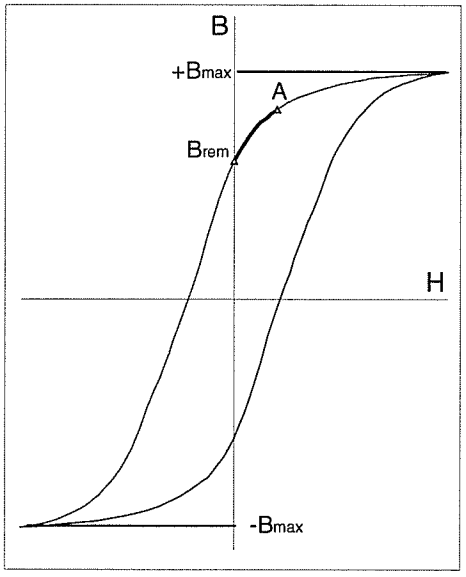

Figure B 2 Hysteresis loop

In a transformer, the voltage over the excited winding is imposed by the power system it is connected to. In the case drawn in Figure B 1, the flux in the core has a value of +Brem at the switch *on* instant. According to Eq. B 1, the derivative of the flux has the same sign

as the voltage sign. This means that the flux will increase in magnitude as long as the voltage is positive, reaching values well within saturation.

Under saturation the current necessary to create such flux density will be several times the nominal current. If the overload and/or differential relays are not properly set up, they could give false trip commands at energization. It is therefore important to have a model that can be used to estimate the inrush phenomena so the overload and/or differential protection relays can be properly set up.

Appendix 3 SINGLE PHASE TRANSFORMER DATA

The construction and electrical parameters of the second transformer modeled in chapter 6 are:

S = 60 MVA	transformer's rated power
n_1 = 87	number of turns in secondary coil (LV)
n_2 = 542	number of turns in primary coil (HV)
r_1 = 6.3 mΩ	secondary winding resistance
r_2 = 0.52 Ω	primary winding resistance
A = 0.534 m^2	area of transformer main core leg
V_1 = 28169 V RMS	low voltage winding nominal line to ground voltage
V_2 = 175546 V RMS	high voltage winding nominal line to ground voltage
Bn = 1.608 T	nominal core flux density at 60 Hz
Lc = 7.5648 m	total equivalent length of core (see Figure C 1)

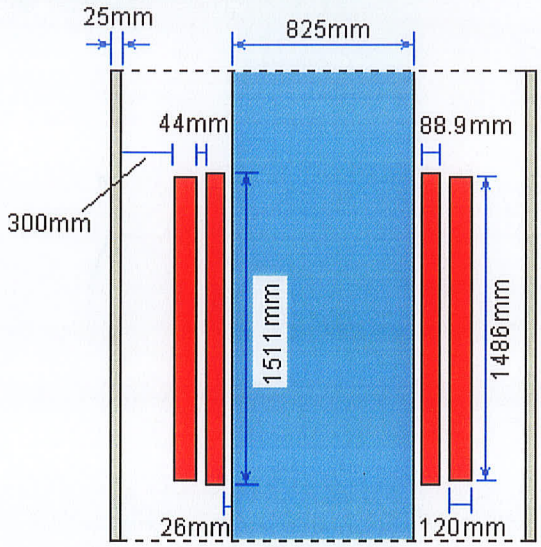

Figure C 1 General layout of the second single-phase transformer studied in chapter 6